Volume 40
Number 6
June 2025
Pages 1421–1604

JAAS

Journal of Analytical Atomic Spectrometry

rsc.li/jaas

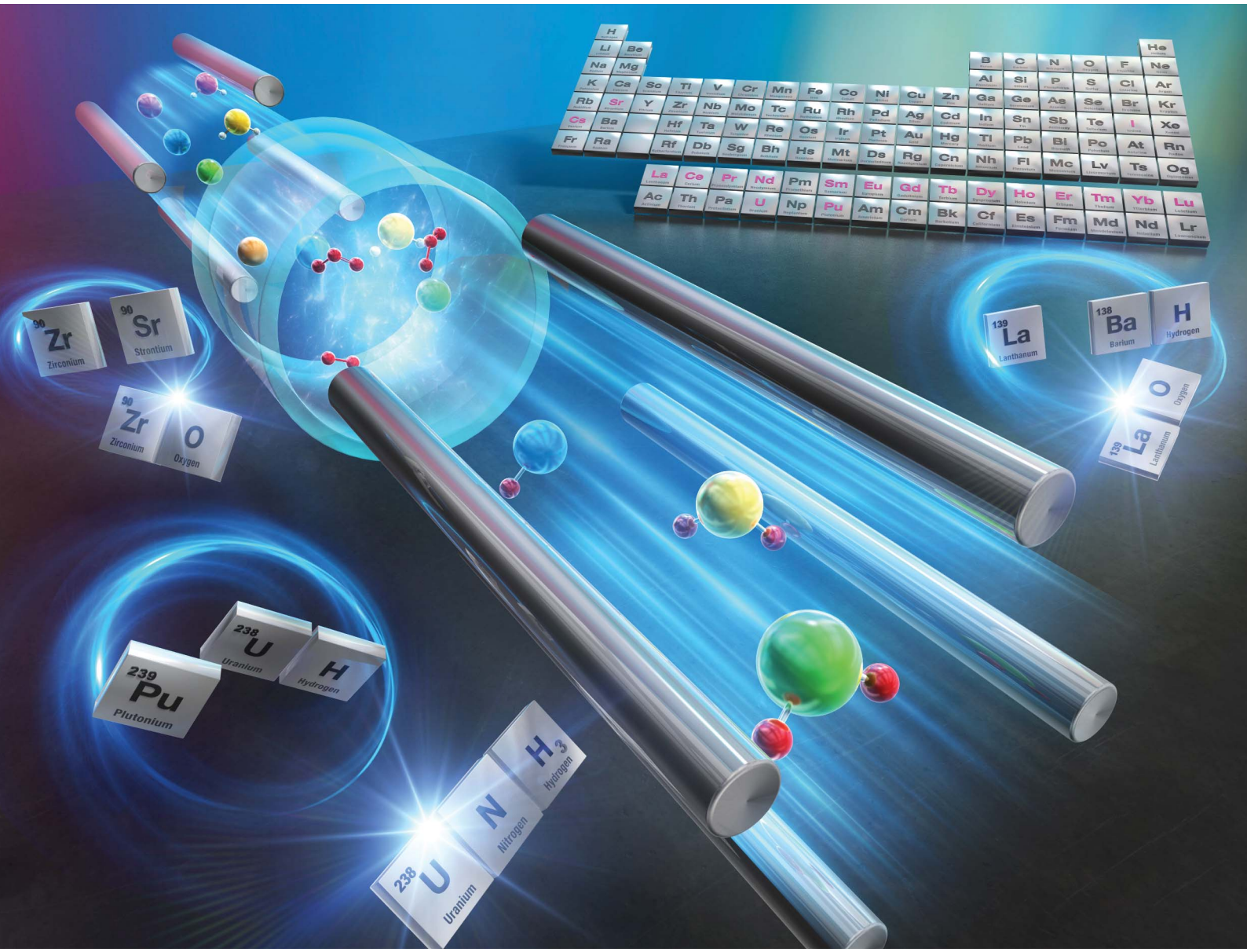

ISSN 0267-9477

ROYAL SOCIETY OF CHEMISTRY

CRITICAL REVIEW

Yanbei Zhu, Jian Zheng *et al.*

Tandem quadrupole inductively coupled plasma mass spectrometry for the quantitative and isotopic analysis of rare earth elements and radionuclides

JAAS

ROYAL SOCIETY OF CHEMISTRY

CRITICAL REVIEW

View Article Online
View Journal | View Issue

Cite this: *J. Anal. At. Spectrom.*, 2025, **40**, 1428

Tandem quadrupole inductively coupled plasma mass spectrometry for the quantitative and isotopic analysis of rare earth elements and radionuclides

Yanbei Zhu, *[a] Guosheng Yang, [b] Aya Sakaguchi, [c] Tsutomu Miura,[a] Yasuyuki Shikamori[ad] and Jian Zheng *[b]

Received 14th November 2024
Accepted 21st February 2025

DOI: 10.1039/d4ja00409d

rsc.li/jaas

Tandem quadrupole inductively coupled plasma mass spectrometry (ICP-QMS/QMS) provides an effective approach for separating spectral interferences without sacrificing the signal intensity due to the increased requirement for mass resolution. This feature is especially important for the analysis of rare earth elements (REEs) and radionuclides, the accurate and precise measurement of which usually suffer from severe spectral interferences. The present review covers the advances and applications of ICP-QMS/QMS in the analysis of rare earth elements and radionuclides reported in around 150 articles since 2012, when the first commercially available ICP-QMS/QMS was released. Specifically, the strategies for separating spectral interferences are highlighted, including chemical separation prior to the analysis, reaction cell technique in ICP-QMS/QMS measurement, and post-analysis mathematical correction. Subsequently, the improvements in the analytical figures of merits are summarized along with the major advancements, focusing on REEs and radionuclides of Cs, I, Sr, U and Pu. Finally, the challenges and potential solutions to address them in future works are presented.

[a]*National Institute of Advanced Industrial Science and Technology, 1-1-1 Umezono, Tsukuba, Ibaraki 305-8563, Japan. E-mail: yb-zhu@aist.go.jp*
[b]*National Institutes for Quantum Science and Technology, 4-9-1 Anagawa, Inage-ku, Chiba-shi 263-8555, Japan. E-mail: zheng.jian@qst.go.jp*
[c]*University of Tsukuba, 1-1-1 Tennodai, Tsukuba, Ibaraki, 305-8577, Japan*
[d]*Tohoku University, 2145-2, Narita-cho, Oarai-machi, Higashiibaraki-gun, Ibaraki 311-1313, Japan*

1 Introduction

Tandem quadrupole inductively coupled plasma mass spectrometry (ICP-QMS/QMS) with a collision/reaction cell (CRC) exhibits excellent performance in elemental and isotopic analysis since its commercial availability in 2012 (initially issued as Agilent 8800 by Agilent Technologies).[1]

Yanbei Zhu

Yanbei Zhu is a Chief Senior Researcher at the National Metrology Institute of Japan (NMIJ) and National Institute of Advanced Industrial Science and Technology (AIST), Japan. Yanbei received his PhD in March 2005 from Nagoya University, where he worked as a Postdoc Fellow from April 2005 to March 2007. He joined NMIJ/AIST in April 2007 and started research on the development of certified reference materials (CRMs) and related techniques for elemental analysis in food and environmental samples. Yanbei's work is focused on quantitative elemental analysis based on ICP-MS-related techniques and the development of devices and instruments for the sample pretreatment process and on-site analysis.

Guosheng Yang

Guosheng Yang obtained his PhD in Bioinorganic Chemistry from the Institute of High Energy Physics, Chinese Academy of Sciences in 2012. He currently works as a Senior Researcher at the National Institutes for Quantum Science and Technology, Japan. His research interests are focused on the method development and application of radiometric and mass spectrometric instruments for radionuclides, especially actinides in environmental and bioassay samples. Owing to his achievement in the field of radionuclide analysis for dose assessment, he received the Young Nuclear Professional-Early Career Award in 2022 and Encouragement Award from the Japan Society of Nuclear and Radiochemical Sciences in 2024.

The powerful ionization capability of high-temperature argon plasma provides high sensitivity for elemental analysis, but it causes severe spectral interferences due to the ionization of argon gas and solvent contents and the coexisting elements in the samples. CRC provides an excellent solution for spectral interference in single quadrupole (SQ-) ICP-MS.[2] However, one of the problems associated with the reaction cell in SQ-ICP-MS is the complexity of reactions occurring in it due to the enormous amount of ionic species generated by the argon plasma. In ICP-QMS/QMS, the introduction of a quadrupole mass filter in front of the CRC limits the ions passing into the CRC, greatly simplifying the reactions between the ions and gas molecules. An ion of interest can be measured in the so-called on-mass mode or mass-shift mode using ICP-QMS/QMS.[2] In the case of on-mass mode measurement, an ion is measured as its initial species by monitoring its initial mass-to-charge ratio (*i.e.* m/z) at the second quadrupole, for which the m/z is set to be identical to that for the first quadrupole (*e.g.* $m/z = 139$ for both quadrupoles to permit the passage of $^{139}La^{+}$). By contrast, in mass-shift mode measurement, the measurement of an ion at the second quadrupole is conducted by monitoring a multi-atomic species generated in the CRC, where the m/z for the second quadrupole is set to a value higher than that for the first quadrupole (*e.g.* $m/z = 139$ and $m/z = 155$ for the first and the second quadrupoles to permit the passage of $^{139}La^{+}$ and $^{139}La^{16}O^{+}$, respectively).

Aya Sakaguchi

Aya Sakaguchi is a Professor of Radiochemistry/Radioscience in the Institute of Pure and Applied Sciences at University of Tsukuba, Japan. She received her PhD (Sci) in 2007 from Kanazawa University. She specializes in the analysis of natural and artificial radionuclides in environmental samples. Samples are collected via field surveys and chemically processed and analysed for target radionuclides using radiometry and mass spectrometry. Her recent work includes challenging topics such as laboratory tracer experiments to elucidate elemental cycling in surface environments using accelerator-produced short half-life radionuclides and spike production for the measurement of long half-life actinides in the environment.

Yasuyuki Shikamori

Yasuyuki Shikamori is an Academic Researcher in the Institute for Materials Research at Tohoku University and in the Geoinformation Research Division of the National Institute of Advanced Industrial Science and Technology (AIST). He received his MSc from Tokyo University of Science in 1988. After engaging in research on trace and ultra-trace elemental analysis techniques for semiconductor and electronic materials at UBE Corporation until 2006, he worked as a Senior Application Chemist at Agilent Technologies until 2022, where he was engaged in hardware and application development. Currently, he is focused on instrument and application development and human resource development for high-sensitivity radionuclide analysis using ICP-MS(/MS) at Tohoku University.

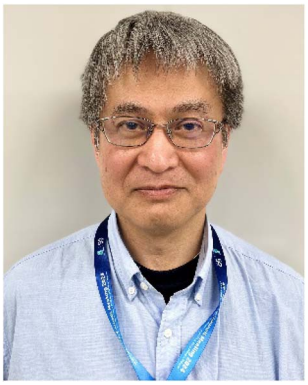

Tsutomu Miura

Tsutomu Miura is a Chief Senior Researcher at the National Metrology Institute of Japan (NMIJ) and National Institute of Advanced Industrial Science and Technology (AIST), Japan. He received his PhD (Sci) from Tokyo Metropolitan University in 2003. His work at NMIJ/AIST is focused on the development of certified reference materials for Inorganic Analysis using classical methods (gravimetric analysis and titration) and instrumental analytical methods (ICP-OES, ICP-MS, and neutron activation analysis).

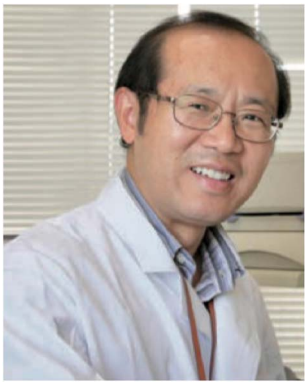

Jian Zheng

Jian Zheng graduated from Fudan University (China) in 1987 and obtained his PhD in Environmental Analytical Chemistry from Karl-Franzens University, Austria in 1998. He currently works as a Senior Principal Researcher at the National Institute for Quantum Science and Technology, Japan. He has published >170 research articles in international journals. His research interests are focused on the development and application of mass spectrometric techniques for trace element/radionuclide speciation, isotope ratio measurement, environmental behavior of radionuclides, and radiation protection. He received an NIRS Research Award in 2009 and the Society Award from the Japan Society of Nuclear and Radiochemical Sciences in 2015.

Lanthanides are usually referred to as rare earth elements (REEs) together with Sc and Y. Although fractionations among REEs occur in the environment, they essentially have similar behavior and are usually found together in natural samples owing to the similarity in their physicochemical properties.[3] As a result, the fractionation of REEs based on their concentration in a sample can help understand its chemical property and history. However, the measurement of heavier (with a larger m/z) REEs (*e.g.* ^{155}Gd and ^{165}Ho) usually suffers from spectral interference of lighter REEs (*e.g.* $^{139}La^{16}O$ and $^{149}Sm^{16}O$, respectively). The application of ICP-QMS/QMS has been shown to be effective to reduce this type of spectral interferences.[1]

Long and medium half-life radionuclides have also attracted significant attention in the application of ICP-QMS/QMS.[4] This can be attributed to its excellent capability for separating spectral interferences. Most radionuclides of interest exist in extremely low concentrations, sometimes even lower than 10^{-10} g mL^{-1} (or g g^{-1}). Consequently, the measurement of these low concentrations of radionuclides by ICP-MS often suffer spectral interferences from much higher concentrations (over 10^6-fold that of radionuclides) of coexisting stable or long-lived radioactive isotopes.

Thus far, numerous reviews have been published on the application of ICP-QMS/QMS; however, none focused on REEs and radionuclides.[2–11] Thus, the present review concentrates on the application of ICP-QMS/QMS for the measurement of REEs and radionuclides published to date. There are two major reasons why we combined REEs and radionuclides in the present work. Firstly, REEs are often studied together with two radionuclides, *i.e.* U and Th; secondly, spectral interferences from co-existing elements/isotopes can be critical in the measurement of both REEs and radionuclides. Accordingly, we hope that readers can find helpful information for future studies on related topics.

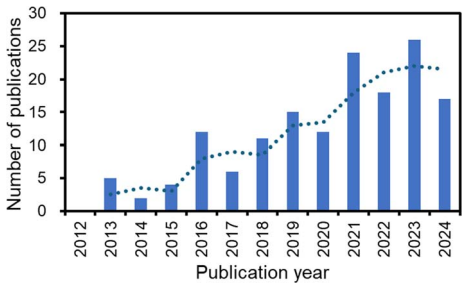

Fig. 1 Trend in the publications on lanthanides and radionuclides measured using ICP-QMS/QMS (dotted line shows the moving average).

2 Trend in publications on ICP-QMS/QMS-based analysis of lanthanides and radionuclides

The trend in the publications (based on the database of Web of Science) on lanthanides and radionuclides measured using ICP-QMS/QMS is illustrated in Fig. 1. Generally, the number of publications has steadily increased since the first ICP-QMS/QMS instrument became commercial availability in 2012. There has been over 15 publications per year since 2021.

This is a profound achievement regarding the limited topics conducted with a single type of ICP-MS.

The publications covered in the present work are summarised in Tables 1–4 for reviews,[2–11] REEs (lanthanides),[1,12–44] RNs (radionuclides),[45–141] and both REEs and RNs,[142–153] respectively. Also, the distribution of publications according to the topics is plotted in Fig. 2.

According to Tables 2–4, it can be seen that the measurement of REEs and RNs by ICP-QMS/QMS has been applied in various research fields, covering material, geological, biological, environmental, and food.

The instrument model is dominated by Agilent 8800 (together with Agilent 8900), which is partially attributed to its early availability since 2012. Alternatively, the application of iCAP TQ and Nexion 5000 has increased since 2021 and 2022, respectively. Considering that these instruments were released in different years (Agilent 8800, 2012; Agilent 8900, 2016; iCAP TQ, 2017; and Nexion 5000, 2020),[9] it can be expected that the application of the latter instruments will increase apparently in the near future.

The most significant advantage of ICP-QMS/QMS is its capability to separate spectral interference, while the effectiveness of the separation depends on the reactions between the ions and gas molecules in the CRC. Therefore, choosing the optimum cell gas (or gas mixture) is an important step to take the advantage of ICP-QMS/QMS.

Table 1 Reviews covering REEs and RNs measured using ICP-QMS/QMS

Publishing year	Sample (topics)	Instrument or method	Ref. no.
2015	Environmental (advances)	Atomic spectrometry	7
2016	Environmental (radionuclides)	Mass spectrometry	6
2018	Environmental (advances)	Atomic spectrometry	8
2018	Multiple matrix (advances)	ICP-QMS/QMS	2
2020	Multiple matrix (radionuclides)	CRC-ICP-MS	4
2021	Geochemical (interference separation)	ICP-MS	5
2021	Multiple matrix (trends and advances)	ICP-QMS/QMS	10
2023	Multiple matrix (REEs)	Analytical techniques	3
2023	Multiple matrix (radionuclides)	Analytical greenness	11
2023	Multiple matrix	ICP-QMS/QMS	9

Table 2 Publications about REEs measured using ICP-QMS/QMS

Publishing year	Sample	Instrument	Ref. no.
2013	Model solution	Agilent 8800	1
2015	Nd oxide	Agilent 8800	12
2015	Nd oxide	Agilent 8800	13
2016	Sediment, soil	Agilent 8800	14
2016	Quartz-rich	Agilent 8800	15
2016	$BaCO_3$	Agilent 8800	16
2017	CRMs[a]	Agilent 8800	17
2018	Bone	Agilent 8800	18
2018	Biological	Agilent 8800	19
2019	Printed circuit boards	Agilent 8800	20
2019	Ce chelates	Agilent 8800	21
2020	Seawater	Agilent 8800	22
2021	Uranium ore	Agilent 8900	23
2021	Uranium ore	iCAP TQ	24
2021	Model solution	Agilent 8900	25
2021	Garnet, apatite, xenotime	Agilent 8900	26
2022	Natural water	Agilent 8900	27
2022	Apatite	Agilent 8900	28
2022	Sediment	Agilent 8800	29
2022	Uranium ore	Agilent 8800	30
2022	La_2O_3 material	iCAP TQ	31
2022	Shales	Not available	32
2022	River water CRMs	Agilent 8800	33
2023	Geological	Agilent 8900	34
2023	Coal	Not available	35
2023	Fertilizer, insect	iCAP TQ	36
2023	Olive oil	Agilent 8800	37
2023	Geological	iCAP TQ	38
2023	Coal ash	iCAP TQ	39
2024	Environmental	Agilent 8800	40
2024	Geological	Agilent 8900	41
2024	Geological	Agilent 8900	42
2024	Seafood	Agilent 8800	43
2024	Silicate	Agilent 8900	44

[a] CRMs, certified reference materials.

The cell gases investigated in the references covered in the present work are summarised in Table 5, together with the number of references for each type of gas. Among them, it can be seen that oxygen (70) is the most investigated cell gas, followed by helium (61) and ammonia gas (34). Hydrogen was also often investigated as a cell gas, which has been reported in 23 references. One of the reasons for using these gases as the cell gas is that they are usually the standard for an ICP-QMS/QMS instrument. It is notable that N_2O (25) and CO_2 (17) were also widely investigated although are not the standard. Also, it is noteworthy that ozone was used as a reaction gas.[141]

2.1 Reaction gases used for measurement of REEs

The typical spectral interferences in the measurement of REEs are monoxide ions of light REEs (LREEs) and those of middle REEs (MREEs) interfere in the measurement of MREEs (*e.g.* $^{139}La^{16}O^+$ with $^{155}Gd^+$) and heavy REEs (HREEs) (*e.g.* $^{147}Sm^{16}O^+$ with $^{163}Dy^+$), respectively. Hydride ions, monoxide ions, and hydroxide ions of Ba also interfere in the measurement of REEs, *e.g.* $^{138}Ba^1H^+$ with $^{139}La^+$, $^{137}Ba^{16}O^+$ with $^{153}Eu^+$, and $^{136}Ba^{16}O^1H^+$ with $^{153}Eu^+$, respectively.

The dominant reaction gas used for REEs was oxygen, which is mainly attributed to its capability to form monoxide for the mass-shift measurement of REEs.[1,12,16–18,20–25,27,35–37,44] However, the yields of monoxides of Eu and Yb (approximately 20%) were much lower than that of other REEs (over 90%) due to their endothermic reaction with oxygen, resulting in deteriorated sensitivity for mass-shift measurement.[22,23,35,53] An improvement in the yield of monoxides of Eu and Yb by two- to three-fold could be achieved *via* optimization of the operating conditions of ICP-QMS/QMS in terms of a higher collision energy.[27] A more reactive gas, N_2O, was also applied in the measurement of REEs in mass-shift mode with higher yields of monoxide ions for the whole set of REEs, including Eu and Yb with yields of over 80%.[32,33,42,44] It is notable that slightly decreased (by 5% to 10%) yields of monoxide ions were found for some REEs (*e.g.* La) due to the formation of dioxide ions.

On-mass mode measurements of REEs with hydrogen[15,16,18,22,29,31,43] or helium[12–16,20,22–24,29,34,36,37,39–43] as the cell gas were reported in multiple works, owing to their ready availability as cell gases or less challenging spectral interferences.

Ammonia gas was also investigated as a cell gas for the measurement of REEs in multiple works.[1,12–14,16,28,34,39,41] It is notable that due to the formation of BaO_2^+ in a high-concentration Ba solution, the on-mass measurement of Eu isotopes with NH_3 reaction resulted in a better performance than the mass-shift measurement with O_2 reaction.[16] Ammonia reaction was the most effective for separating signals of Lu and Hf for their isotopic analysis, where Lu could be measured in the on-mass mode and Hf in the mass-shift mode of ion clusters of Hf with NH_3.[26,28,34,41]

2.2 Reaction gases used for the measurement of radionuclides of Cs

The measurement of ^{134}Cs is extremely difficult because it is a short-lived radionuclide. As alternatives, radionuclides of Cs, *i.e.* ^{135}Cs and ^{137}Cs, have been studied to evaluate its environmental effects due to nuclear power- or nuclear weapon-related activities. Isobaric spectral interferences from $^{135}Ba^+$ and $^{137}Ba^+$ should be considered in the measurement of trace $^{135}Cs^+$ and $^{137}Cs^+$ by ICP-MS, respectively. The most effective reaction gas for the measurement of radionuclides of Cs was N_2O, which helped transform Ba ions effectively to their oxide or hydroxide ions.[48,49,51,52,54,56,57,84,100,101]

The additional application of NH_3 (in He) helped remove polyatomic interferences from $^{119}Sn^{16}O^+$, $^{95}Mo^{40}Ar^+$, $^{97}Mo^{40}Ar^+$, and $^{121}Sb^{16}O^+$.[119,120]

2.3 Reaction gases used for the measurement of radionuclides of Sr

As an analog of calcium, Sr has a tendency to accumulate in the skeleton after its intake by human beings. Therefore, radionuclides of Sr have attracted significant attention as a threat to human health. In this case, ^{90}Sr, which poses a great threat to human health, is often determined by ICP-MS. However, the measurement of $^{90}Sr^+$ suffers spectral interferences from mainly $^{90}Zr^+$ and $^{89}Y^1H^+$.

Table 3 Publications on RNs measured using ICP-QMS/QMS

Publishing year	Sample	Instrument	Isotope of interest	Ref. no.
2013	Model solution	Agilent 8800	I-129	46
2013	Soil	Agilent 8800	Sr-90	45
2013	Model solution	Agilent 8800	U-236, 238	47
2013	Soil	Agilent 8800	I-129	135
2014	Rain water	Agilent 8800	Cs-134, 135, 137	48
2014	Environmental	Agilent 8800	Cs-135, 137	49
2015	Cigar tobacco	Agilent 8800	U-238	50
2016	Model solution	Agilent 8800	U-236, 238	53
2016	Soil and sediment	Agilent 8800	Sr-90, Cs-137; Pu-238, 239, 240	51
2016	River suspended particles	Agilent 8800	Cs-135, 137; Pu-239, 240	52
2016	Environmental	Agilent 8800	Cs-135, 137	55
2016	Environmental	Agilent 8800	U-236, 238	54
2016	Environmental	Agilent 8800	Cs-135, 137	56
2016	Environmental	Agilent 8800	Cs-135, 137	57
2017	Decommission waste	Agilent 8800	Sr-90	58
2017	Atmospheric particulate matter	Agilent 8800	Sr-90	59
2017	Groundwater and discharge water	Agilent 8800	Ra-226	60
2017	Soil	Agilent 8800	U-236, 239, 240	61
2018	Mo powder	Agilent 8800	Th-232, U-238	62
2018	Vegetation	Agilent 8800	U-234, 235, 238	63
2018	Seawater	Agilent 8800	U-238	64
2018	Model solution	Agilent 8900	U-238; Np-237; Pu-240; Am-241; Cm-244	65
2018	Environmental	Agilent 8800	Pu-239, 240	66
2018	Environmental	Agilent 8800	I-129	136
2019	Environmental and forensic	Agilent 8800	Pu-239	68
2019	Soil and sediment	Agilent 8800	U-236	69
2019	Soil	Agilent 8800	U-236	70
2019	CRM	Agilent 8900	Pu-238	71
2019	Urine	Agilent 8800	Sr-90	72
2019	Nuclear waste	Agilent 8800	Cl-36; Ca-41; Ni-59, 63; Se-79; Sr-90; Zr-93; Nb-94; Tc-99; Pd-107; Sn-126; I-129; Cs-135, 137; Pm-147; Sm-151; Pu-239; Am-241	73
2019	CaF_2 sludge	Agilent 8800	U-234, 235, 238	74
2019	Soil	Agilent 8800	I-129; Cs-134, 137	75
2019	Soil and sediment	Agilent 8800	Cs-134, 137; U-234, 235, 238	76
2019	Soil	Agilent 8800	Pu-239, 240	77
2020	Uranium CRM	Agilent 8800	U-234, 238	67
2020	Mining residues	Agilent 8900	U-234, 235, 238; Th-230, 232; Ra-226, 228; Pb-210	78
2020	Environmental	Agilent 8800	U-236, 238	79
2020	Environmental water	Not available	Pu-239, 240	80
2020	Environmental	Agilent 8800	U-236, 238	81
2020	Kaolinitic	Agilent 8800	U-234, 235, 238; Th-230, 232	82
2020	Medicinal herbs	Agilent 8800	Th-232; U-238	83
2020	Environmental	Agilent 8800	Cs-135, 137	84
2021	Environmental	Agilent 8800	U-236	85
2021	Environmental	Agilent 8900	Pu-239, 240	86
2021	Bone	Agilent 8800	U-238	87
2021	Reference materials	Agilent 8900	U-233, 235, 238	88
2021	Uranium material	Not available	Th-232	89
2021	Model solution	Agilent 8800 Agilent 8900	Cl-36; Ca-41; Ni-63; Mo-93	90
2021	Concrete	Agilent 8800	Ca-41	91
2021	Lake water, seawater, urine	Agilent 8800	Sr-90; U-234; Am-241; Pu-239	92
2021	Liquid sample with complex matrices	Agilent 8800	Sr-90	93
2021	Environmental samples	Agilent 8800	U-236	94

Table 3 (*Contd.*)

Publishing year	Sample	Instrument	Isotope of interest	Ref. no.
2021	Urine	Agilent 8900	Pu-239, 240	95
2021	Soil	Agilent 8800	Pu-239	96
2021	Urine	Agilent 8800	Np-237; Pu-239, 240, 241	97
2021	Soil	Agilent 8900	Pu-239	98
2021	Soil, sediment	Agilent 8800	Am-241	99
2021	Waste samples	Agilent 8800	Cs-135, 137	100
2021	Environmental samples	Agilent 8900	Cs-135, 137	101
2022	Model solution	Agilent 8900	Tc-99	102
2022	Lead metal	Agilent 8800	Pu-239, 242	103
2022	Soil, sediment	Agilent 8900	Cs-135, 137	104
2022	Model solution	Nexion 5000	I-129	105
2022	Model solution	Nexion 5000	Pu-239, 240, 241, 242, 244	106
2022	Water	Not available	Th-230, 232; U-234, 235, 238	107
2022	Atmospheric deposition	Agilent 8800	U-235, 236, 238	108
2022	Soil, sediment	Agilent 8900, Nexion 5000	Pu-239, 240, 241	109
2022	Environmental samples	Agilent 8900	Tc-99	110
2022	Soil	Agilent 8900	Am-241	111
2022	Environmental	Agilent 8900	I-129	138
2023	Cotton swipes	iCAP TQ	U-234, 235, 236, 238; Pu-239, 240	112
2023	Environmental gaseous samples	Agilent 8900	I-129	113
2023	Soil	Agilent 8900	Pu-239, 240	114
2023	Soil	Agilent 8800	Np-237; Pu-239, 240	115
2023	High U sample	Agilent 8800	Pu-238, 239, 240, 241	116
2023	Environmental samples	Agilent 8900	U-236, 238	117
2023	Standard	Agilent 8900	Np-237; Am-241; Cm-244	118
2023	Soil and sediment	Agilent 8900	Cs-135, 137	119
2023	Environmental samples	Agilent 8900	Cs-135, 137	120
2023	Water	Agilent 8900	Pu-239, 240	121
2023	Multiple matrix	Agilent 8800	Ni-63; Sr-90; Zr-93; Tc-99; I-129; Np-237; Pu-239	122
2023	Sediment samples	Agilent 8900	Am-241	124
2023	Urine	Agilent 8800	U-234, 235, 238; Pu-239, 240, 241	125
2023	Urine	Agilent 8900	Sr-90	137
2023	Soil	Agilent 8800	Np-237; Pu-239, 240	126
2023	Gd sulfate octahydrate	Agilent 8800	Ra-226	123
2023	Wild boars	Agilent 8900	Cs-135, 137	139
2023	Urine	Agilent 8800	Sr-90	137
2023	Decommissioning waste	Agilent 8800	I-129	140
2024	Model solution	Agilent 8900	U-238; Pu-238, 239	127
2024	Environmental samples	Agilent 8900	Pu-239	128
2024	Metal sample	Agilent 8800	Th-230	130
2024	Urine	Agilent 8900	Np-237; Pu-239, 240, 241; Am-241; Cm-244	131
2024	Bottled drinking water	Agilent 8900	Po-210; Ra-226, 228; Th-230, 232; U-234, 235, 236	132
2024	Uranium ore	Agilent 8800	Th-230, 232; U-234	133
2024	Biological samples	Agilent 8800	Pu-239, 240	134
2024	Scintillation film	Agilent 8800	Th-232; U-238	129
2024	Natural water	Agilent 8800	I-129	141

Oxygen is effective in removing the interference from $^{90}Zr^+$ by transforming it to its oxide ions.[45,51,58,72,92,93,122] Recently, Yang *et al.* demonstrated that the introduction of CO_2 instead of O_2 could further mitigate isobaric/polyatomic interferences, especially that caused by Zr and Ge.[137]

Additionally, the application of H_2 and NH_3 resulted in the best performance for the measurement of $^{90}Sr^+$ by separating Zr- and Y-related spectral interferences.[59]

2.4 Reaction gases used for the measurement of radionuclide of I

Anthropogenic ^{129}I is attracting attention as a geochemical tracer related to nuclear weapons testing, nuclear accidents, nuclear reprocessing facilities, and nuclear power plants.[46,75,105,113,135,136,138,140,141] The measurement of $^{129}I^+$ by ICP-QMS/QMS suffers spectral interferences from $^{129}Xe^+$ and $^{127}I^1H_2^+$.

Table 4 Publications on REEs and RNs measured using ICP-QMS/QMS

Publishing year	Sample	Instrument	Element or isotope of interest	Ref. no.
2017	River water, spring water	Agilent 8800	REEs; Th-232; U-238	144
2019	Arctic samples	Agilent 8900	REEs; U-238	145
2019	Sediment	Agilent 8800	REEs; Th-232; U-238	147
2019	Water and sediment	Agilent 8800	REEs; Th-232; U-238	150
2020	Sediment	Agilent 8800	REEs; Th-232; U-238	153
2021	CMX-6	Agilent 8800	REEs; U-234, 235, 236, 238; Pu-239, 241, 242	143
2021	Sediment	Agilent 8800	REEs; U-238	148
2022	Water CRMs	Agilent 8800, Agilent 8900	REEs; Th-232; U-238	142
2023	Water	Agilent 8900	REEs; U-238	146
2023	Plant SRMs	Nexion 5000	REEs; Th-232; U-238	152
2024	Sediment	Agilent 8800	REEs; U-238	149
2024	Wheat flour	Agilent 8800	REEs; Th-232; U-238	151

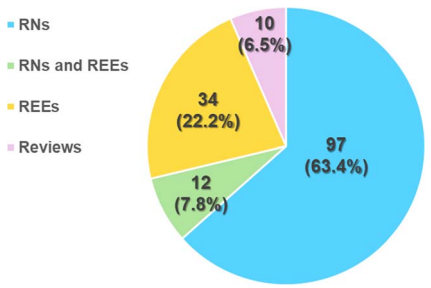

Fig. 2 Distribution of publications according to the topics of lanthanides (REEs), radionuclides (RNs), both (RNs and REEs), and reviews.

Table 5 Collision and reaction gases investigated *via* ICP-QMS/QMS measurement

Gas	References	Count
He	13–16, 20, 22–24, 28, 29, 34, 36, 37, 39, 40, 42, 43, 49, 60, 65, 67, 68, 73, 74, 81, 83, 86, 89–92, 94, 96, 98, 101, 102, 107, 111, 112, 115, 116, 119–122, 124–126, 131–133, 142, 144–151 and 153	61
H_2	15, 16, 18, 22, 29, 31, 43, 51, 58, 59, 65, 71, 73, 90–93, 122, 143, 144, 146, 147 and 153	23
O_2	1, 12, 13, 15–18, 20–25, 27, 35, 36, 39, 44–47, 51, 53, 55, 58, 59, 62, 65, 67–70, 72, 73, 75, 76, 78, 79, 81, 85, 92, 93, 98, 102, 105, 106, 108, 110, 111, 113, 114, 116–118, 121, 122, 124, 127, 131, 135, 136, 138, 140, 142, 144, 145, 147–149 and 153	70
NH_3	1, 12–14, 16, 21, 25, 26, 28, 34, 39, 41, 51, 58, 59, 62, 66–68, 73, 77, 86, 90, 91, 95, 96, 99, 109, 116, 119, 120, 122, 134 and 144	34
N_2O	29, 32, 33, 42–44, 48, 49, 51, 52, 54, 56, 57, 81, 84, 100, 101, 116, 117, 119, 120, 127, 138, 139 and 152	25
CH_4	51	1
C_2H_2	51	1
CO_2	51, 68, 71, 79, 81, 94, 98, 105, 106, 112, 115, 116, 118, 127, 137, 138 and 143	17
NO	106 and 128	2
O_3	141	1

Oxygen was used in most works for measuring $^{129}I^+$ by ICP-QMS/QMS, while on-mass measurement was selected to remove $^{129}Xe^+$ and $^{127}I^1H_2^+$ as their products from reactions with O_2.[46,75,105,113,135,136,140] Matsueda *et al.* tried to improve the analytical performance for the on-mass measurement of $^{129}I^+$ using CO_2 in addition to O_2 as the reaction gas.[105]

Coralie *et al.* compared N_2O, CO_2 and O_2 as the reaction gas for the mass-shift measurement of $^{129}I^+$ as its monoxide ion.[138] Among them, the best analytical performance was achieved with O_2, resulting in a yield of approximately 15% of monoxide ion of $^{129}I^+$.

In a recent study by Zhu and Asakawa, they used on-line-generated ozone (O_3) as the reaction gas for the mass-shift measurement of $^{129}I^+$.[141] Due to its spontaneous reaction with O_3, $^{129}I^+$ could be measured as its monoxide ion and dioxide ion with yields of approximately 60% and 20%, respectively.

2.5 Reaction gases used for the measurement of radionuclides of U

In addition to long-lived radionuclides of uranium (^{235}U and ^{238}U), anthropogenic and relatively shorter-lived radionuclides (*e.g.* ^{233}U, ^{234}U, and ^{236}U) have been increasingly measured by ICP-QMS/QMS for the investigation of nuclear-related environmental activities. In most cases, interference from $^{235}U^1H^+$ in the measurement of $^{236}U^+$ was the major challenge due to the relatively higher abundance (*ca.* 0.7%) of ^{235}U in comparison to the extremely low natural abundance (usually under 10^{-5}%) of ^{236}U. Oxygen was mostly investigated as the reaction gas for the measurement of uranium isotopes by shifting to their monoxide ions.[47,54,67,70,79,81,85,92,108,117] Beside oxygen, CO_2 and N_2O were investigated as alternative gases for the measurement of uranium isotopes.[79,81,94,112,117] The introduction of N_2O as the reaction gas permitted the measurement of uranium isotopes by shifting to their dioxide ions and helped improve the spectral interference separation.[117]

Helium was usually used as an additional gas with oxygen, CO_2, and N_2O, helping to improve the reactions by enhancing the collision opportunities.[67,74,78,79,81,92,94,107,112,125,132,133]

2.6 Reaction gases used for the measurement of radionuclides of Pu

Due to their high radiological toxicity and very long radioactive half-life, Pu isotopes are regarded as highly hazardous contaminants in the environment, and the most frequently monitored Pu isotopes are those with an isotopic mass of 238 to

241 and 244. In addition to the tailings of a high concentration of ^{238}U, the major spectral interferences were from ^{238}U-related polyatomic and isobaric ions, *e.g.* $^{238}U^1H^+$ and $^{238}U^1H_2^+$. Polyatomic ions from other elements (Pb, Hg, and Tl) should also be considered regarding the sample matrix.[92,98,103]

The dominant reaction gases used for the measurement of Pu isotopes were NH_3,[51,66,77,80,86,95,96,103,109,116,134] CO_2,[51,68,71,106,112,115,127,143] and O_2,[65,98,114,121,122,131] respectively. It is notable that CO_2 was used more often than O_2, regardless of the fact that O_2 is one of the standard reaction gases for ICP-QMS/QMS independent of its manufacturer. This can be attributed to the fact that the measurements of Pu isotopes were conducted in on-mass mode with the polyatomic spectral interferences reduced by reaction with the gas molecules. The reactions with NH_3 and CO_2 resulted in the better removal of these spectral interferences and provided a better performance for the measurement of Pu isotopes.

3 Advances in sample pretreatment

In the analysis of solid samples, acid digestion (or acid leaching) and alkaline fusion are often conducted to transform solid samples to solutions. Also, a limited number of works reported the application of laser ablation on solid samples.[26,28,32,34,130,143]

Due to the extremely low concentrations (usually under ng kg^{-1} or ng L^{-1}) of REEs and RNs in natural samples, pretreatment for the enrichment of the objective element and/or separating it from the sample matrix is usually required prior to measurement by ICP-QMS/QMS.

3.1 Pretreatment for the measurement of REEs

The use of solid-phase extraction (SPE),[14,23,142] cloud point extraction,[14] solvent extraction,[21] and coprecipitation[22] has been reported for the pretreatment of samples to measure REEs.

Ebeling *et al.* reported an automatic SPE method based on a commercially available on-line system (with Nobias chelate-PA1 column, ethylene diamine triacetate and imino-diacetate functional groups), achieving a preconcentration factor of 20 for trace elements including REEs in natural water samples.[142]

Ding *et al.* reported an SPE method using UTEVA resin (diamyl amylphosphonate) for separating REEs from the matrix of uranium ore. The recovery for each REE was over 93% with an acceptable concentration (<100 ng mL^{-1}) of uranium in the final solution.[23]

Labrecque *et al.* compared cloud point extraction and SPE for separation of REEs in isotopic analysis.[14] Regardless the fact that both methods were based on an extractive ligand of diglycol amide analogues, the cloud point extraction method showed excellent recoveries (over 99%) for Nd, Sm, and Eu, which were superior to that obtained with the SPE method (45% to 68%).

Zhang *et al.* reported a solvent extraction method for the determination of REE impurities in Ce chelates.[21] REEs were extracted in bis(2,4,4-trimethylpentyl)phosphinic acid at pH 4 (with the oxidation of Ce by $KMnO_4$), and then back extracted with 5% (v/v) HNO_3. A matrix separation efficiency of over 99.9% was achieved with good reproducibility, resulting in a Ce concentration under 0.1 mg L^{-1} remaining. The recoveries of other REEs were over 90%.

Zhu reported an $Mg(OH)_2$ coprecipitation method for the determination of REEs in seawater samples.[22] An enhancement factor of 130-fold (peak height of signal intensity) was achieved by on-line elution and measurement of the precipitate, with the removal of over 99% salt contents.

3.2 Pretreatment for the measurement of radionuclides of Cs

The selective adsorption of Cs with ammonium molybdophosphate (AMP) was reported in multiple works, followed by further ion-exchange separation to remove the sample matrix and interfering elements.[49,56,57,80,84,101,104,120]

Zheng *et al.* reported an improved method for the removal of major elements (*e.g.* Ca, K, and Mg) following AMP adsorption.[57] Combining a 2 mL AG MP-1M resin (anion exchange) column, a 10.5 mL AG 50W-X8 resin-packed Eppendorf pipette, and 2 mL Sr resin cartridge, sufficient removal of the matrix elements and interfering elements was achieved for the analysis of low-level ^{137}Cs (20–1000 Bq kg^{-1}) using large-size samples (*e.g.* up to 40 g soil and sediment samples). This separation method showed high separation factors (10^4–10^7) for the major matrix elements (Al, Ca, K, Mg, Na and Si) and interfering elements (10^5–10^6 for Ba, 10^6–10^7 for Mo, 10^4–10^6 for Sb and 10^4–10^5 for Sn).

It is notable that a desolvation system helped improve the signal intensity in the measurement by ICP-QMS/QMS, which was attributed to the uptake efficiency of Cs isotopes in the plasma.[57,80,84,120]

3.3 Pretreatment for the measurement of radionuclides of Sr

An automated online SPE method employing a lab-on-valve system was developed for the analysis of ^{90}Sr.[92,93] A dual-column setup (Eichrom DGA resin and Sr resin) helped separate ^{90}Sr from ^{90}Zr and other matrix elements, where the DGA resin had diglycolamic acid functional groups for the extraction of cations.

Strontium in urine samples was efficiently separated by phosphate co-precipitation, followed by extraction chromatography with Pre-filter resin, Eichrom TRU resin (having carbamoylphosphine oxide functional groups), and Sr resin (having 4,4′(5′)-di-*t*-butylcyclohexano 18-crown-6 functional groups).[72] This method enabled the determination of 1 Bq ^{90}Sr per urine sample (1–2 L) for assessing the internal exposure of workers in a radiological emergency. Yang *et al.* applied DGA and Sr resin cartridges for the separation of Sr, following CaF_2 co-precipitation in 400 mL urine samples. In this study, stable ^{88}Sr was used as a yield tracer for the recovery correction of ^{90}Sr.[137]

3.4 Pretreatment for measurement of radionuclide of I

In the work by Ohno *et al.*, ^{129}I in soil samples was released using a V_2O_5-based pyrohydrolysis process and trapped in a solution of 1% TMAH and 0.1% Na_2SO_3. Further purification

was conducted by solvent extraction and back extraction using carbon tetrachloride, $NaNO_2$, HNO_3, and Na_2SO_3.[135]

In the work by Carrier *et al.*, environmental gaseous ^{129}I trapped in a charcoal cartridge was purified with an SPE method after acid digestion.[113] The SPE method was based on Ag^+-functionalized CL resin, which retained iodide as AgI. The elution of ^{129}I was achieved with a solution of 0.35 mol per L Na_2S.

Yang *et al.* reported a multi-step mild extraction protocol for measuring ^{129}I in solid environmental samples.[136] The first step was extraction with 10% TMAH at 90 °C, and the second step was using $K_2S_2O_8$ for releasing iodine from organic matter. In the third step, the reduction of iodate was conducted using $(NH_4)_2SO_3$ with the assistance of CCl_4. After the removal of the organic layer in step four, iodine was extracted with $NaNO_2$ in step five. The final step was back extraction with $(NH_4)_2SO_3$.

Zacharauskas *et al.* used a simple combustion process at 900 °C, followed by trapping with 3% TMAH solution for measuring ^{129}I in nuclear waste simulant samples.[140]

3.5 Pretreatment for the measurement of radionuclides of U

SPE methods using multiple resins were reported as pretreatment for the measurement of radionuclides of uranium. The most used resin was UTEVA, which showed efficiency for the extraction of nitrato complexes of actinide elements.[63,69,79,81,82,94,107,108,117]

Also, other resins were reported as pretreatment for the measurement of radionuclides of uranium, including AG1X8 (a strong cation exchange resin),[69,74,79] DGA,[54,61,70,76,85,92,125] and TRU resins.[78,132]

3.6 Pretreatment for the measurement of radionuclides of Pu

Coprecipitation was reported as pretreatment for the measurement of radionuclides of Pu.[68,77,80,95,109,115,116,126,154] The enrichment and/or separation of Pu were usually conducted with SPE methods using various resins, *e.g.* TEVA resin (with aliphatic quaternary amine functional groups),[51,66,68,77,80,95,96,114,126] TK200 resin (with trioctylphosphine oxide functional groups),[86,115,116,121,126] Sr resin,[92,103] DGA resin,[92,131] AG MP-1M resin (anion exchange),[95–97] AG 1X4 resin (anion exchange),[66,109] and UTEVA resin.[98]

4 Improvement in separating spectral interferences by reaction-cell techniques

The performance of ICP-QMS/QMS in separating spectral interferences depends on the extent of the reactions between the ions and gas molecules in the CRC. On-mass measurements are usually conducted when the reactions between the interfering ions and gas molecules proceed readily, while the ions of interest are much less reactive with the gas molecules. Alternatively, mass-shift mode measurements are conducted in the opposite case.

4.1 Pitfalls and advantages of measurement modes and reaction gases

On-mass measurements basically permit the passing of a relatively lower mass monoatomic ion through the CRC and the second quadrupole before arriving at the detector, while a higher mass polyatomic ion is blocked *via* energy discrimination. For this purpose, a positive or neutral voltage is often applied to the exit of the CRC, resulting in a "repulsion effect" to the positively charged ions. The transmission of the ion of interest decreases due to the increased collisions with the cell gas. The sensitivities for most elements measured in on-mass mode with H_2 reaction were approximately 30% to 60% of that obtained under no-gas condition.[155]

The operating conditions for mass-shift mode measurement benefit the passing of a relatively higher mass polyatomic ion to the detector, with a negative voltage applied to the exit of the CRC, helping to improve the transmission of the ion of interest. In this case, the sensitivity depends on the yield of the polyatomic ion. The sensitivities for most elements measured in mass-shift mode with O_2 ($M^+ \rightarrow MO^+$) and NH_3 ($M^+ \rightarrow MNH^+$) were under 50% and 20%, respectively, of that obtained under no-gas condition.[155]

The systematic characterization of the gas cell reactions using NO, N_2O and O_3 was also reported, respectively.[155–157] These works provide greatly valuable information for further development in the analysis of REEs and radionuclides.

4.2 Representative reaction gases and reactions applied in the measurement of REEs and radionuclides

The representative gas and reactions used for the measurement of REEs and radionuclides of Cs, Sr, U, and Pu are summarized in Table 6, together with the interfering ions and measurement mode.

The measurements of REEs were dominated by the mass-shift mode with O_2 or N_2O as the reaction gas. It is notable that the introduction of N_2O as the reaction gas significantly improved the formation of monoxide ions of Eu and Yb, permitting the mass-shift measurements of a full set of REEs at high sensitivity.

The measurements of radionuclides of Cs were conducted in on-mass mode. The reactive property of N_2O helps completely transform the interfering Ba ions to their oxide ions and break polyatomic ions of Sn, Sb, and Mo. The additional application of NH_3 helped completely remove interferences from these polyatomic ions. The measurement of ^{90}Sr was also conducted in on-mass mode utilizing O_2 or CO_2 (or with additional H_2 and NH_3) as the reaction gas. The on-mass and mass-shift measurements of ^{129}I were often conducted with O_2 as the reaction gas, while its monoxide ion was permitted to pass the second quadrupole for mass-shift measurement.

The measurements of radionuclides of U were conducted in mass-shift mode with O_2, CO_2, or N_2O as the reaction gas. The shifting to oxides of $^{236}U^+$ helped separate it from the interfering $^{235}U^1H^+$, which also shifted to the related oxides.

The measurements of radionuclides of Pu were conducted in mass-shift mode by shifting to oxide ions with O_2 or NO as the

Table 6 Representative improvements in the separation of spectral interferences

Ion of interest	Interfering ions	Reaction gases	Measuring mode	Typical reactions	References
$^{139}La^+$	$^{138}Ba^1H^+$	H_2	On-mass	$^{138}Ba^1H^+ \rightarrow {}^{138}Ba^+$	18 and 31
$^{151}Eu^+$	$^{135}Ba^{16}O^+$			$^{135}Ba^{16}O^+ \rightarrow {}^{138}Ba^+$	
$^{169}Tm^+$	$^{153}Eu^{16}O^+$			$^{153}Eu^{16}O^+ \rightarrow {}^{138}Ba^+$	
$^{139}La^+$	$^{138}Ba^1H^+$	O_2	Mass-shift	$^{139}La^+ \rightarrow {}^{139}La^{16}O^+$	1, 12, 17, 18, 20–25, 27, 35, 36 and 44
$^{151}Eu^+$	$^{135}Ba^{16}O^+$			$^{151}Eu^+ \rightarrow {}^{151}Eu^{16}O^+$	
$^{169}Tm^+$	$^{153}Eu^{16}O^+$			$^{169}Tm^+ \rightarrow {}^{169}Tm^{16}O^+$	
$^{176}Lu^+$	$^{176}Hf^+$	NH_3	On-mass	$^{176}Hf^+ \rightarrow {}^{176}Hf^{14}N_5{}^1H_{12}{}^+$	26
$^{139}La^+$	$^{138}Ba^1H^+$	N_2O	Mass-shift	$^{139}La^+ \rightarrow {}^{139}La^{16}O^+$	32, 33, 42 and 44
$^{151}Eu^+$	$^{135}Ba^{16}O^+$			$^{151}Eu^+ \rightarrow {}^{151}Eu^{16}O^+$	
$^{169}Tm^+$	$^{153}Eu^{16}O^+$			$^{169}Tm^+ \rightarrow {}^{169}Tm^{16}O^+$	
$^{135}Cs^+$	$^{135}Ba^+$	N_2O	On-mass	$^{135}Ba^+ \rightarrow {}^{135}Ba^{16}O^+$	48, 49, 51, 52, 54, 56, 57, 84, 100, 101, 119 and 120
$^{137}Cs^+$	$^{137}Ba^+$			$^{137}Ba^+ \rightarrow {}^{137}Ba^{16}O^+$	
$^{135}Cs^+$	$^{119}Sn^{16}O^+$, $^{95}Mo^{40}Ar^+$	N_2O, NH_3	On-mass	$^{119}Sn^{16}O^+ \rightarrow {}^{119}Sn^+$; $^{95}Mo^{40}Ar^+ \rightarrow {}^{95}Mo^+$	119 and 120
$^{137}Cs^+$	$^{121}Sb^{16}O^+$, $^{97}Mo^{40}Ar^+$			$^{121}Sb^{16}O^+ \rightarrow {}^{121}Sb^+$; $^{97}Mo^{40}Ar^+ \rightarrow {}^{97}Mo^+$	
$^{90}Sr^+$	$^{90}Zr^+$, $^{89}Y^1H^+$	O_2	On-mass	$^{90}Zr^+ \rightarrow {}^{90}Zr^{16}O^+$; $^{89}Y^1H^+ \rightarrow {}^{89}Y^{16}O^+$	45, 51, 58, 59, 72, 92, 93 and 122
$^{90}Sr^+$	$^{90}Zr^+$, $^{89}Y^1H^+$	O_2, CO_2	On-mass	$^{90}Zr^+ \rightarrow {}^{90}Zr^{16}O^+$, $^{90}Zr^{16}O_3{}^+$, $ZrH_{3-4}O_3{}^+$, $ZrH_2O_2{}^+$	137
$^{90}Sr^+$	$^{90}Zr^+$, $^{89}Y^1H^+$	O_2, H_2, NH_3	On-mass	$^{90}Zr^+ \rightarrow {}^{90}Zr^{16}O^{14}N_4{}^1H_{12}{}^+$; $^{89}Y^1H^+ \rightarrow {}^{89}Y^{16}O^{14}N_4{}^1H_{12}{}^+$	59
$^{129}I^+$	$^{129}Xe^+$, $^{127}I^1H_2{}^+$	O_2 (or with CO_2)	On-mass	$^{129}Xe^+ \rightarrow {}^{129}Xe$, $^{127}I^1H_2{}^+ \rightarrow {}^{127}I^+$	46, 75, 105, 113, 135, 136 and 140
$^{129}I^+$	$^{129}Xe^+$, $^{127}I^1H_2{}^+$	O_2	Mass-shift	$^{129}I^+ \rightarrow {}^{129}I^{16}O^+$	138
$^{129}I^+$	$^{129}Xe^+$, $^{127}I^1H_2{}^+$	O_3	Mass-shift	$^{129}I^+ \rightarrow {}^{129}I^{16}O^+$; $^{129}I^+ \rightarrow {}^{129}I^{16}O_2{}^+$	141
$^{236}U^+$	$^{235}U^1H^+$	O_2	Mass-shift	$^{235}U^1H^+ \rightarrow {}^{235}U^{16}O^+$; $^{236}U^+ \rightarrow {}^{236}U^{16}O^+$	47, 54, 67, 70, 79, 81, 85, 92, 108 and 117
$^{236}U^+$	$^{235}U^1H^+$	O_2, CO_2	Mass-shift	$^{235}U^1H^+ \rightarrow {}^{235}U^{16}O^+$; $^{236}U^+ \rightarrow {}^{236}U^{16}O^+$	79 and 94
$^{236}U^+$	$^{235}U^1H^+$	N_2O	Mass-shift	$^{235}U^1H^+ \rightarrow {}^{235}U^{16}O_2{}^+$; $^{236}U^+ \rightarrow {}^{236}U^{16}O_2{}^+$	81 and 117
$^{239}Pu^+$	$^{238}U^1H^+$	O_2 (with H_2 or He)	Mass-shift	$^{239}Pu^+ \rightarrow {}^{239}Pu^{16}O_2{}^+$; $^{238}U^1H^+ \rightarrow {}^{238}U^{16}O_2{}^+$	65, 98, 114, 121, 122 and 131
$^{239}Pu^+$	$^{238}U^1H^+$	CO_2 (with H_2 or He)	On-mass	$^{238}U^1H^+ \rightarrow {}^{238}U^{16}O^+$, $^{238}U^{16}O_2{}^+$	51, 68, 71, 106, 112, 115, 127 and 143
$^{239}Pu^+$	$^{238}U^1H^+$	NH_3	On-mass	$^{238}U^1H^+ \rightarrow {}^{238}U^{14}N^1H_{0-3}{}^+$	51, 66, 77, 80, 86, 95, 96, 103, 109, 116 and 134
$^{239}Pu^+$	$^{238}U^1H^+$	NO	Mass-shift	$^{239}Pu^+ \rightarrow {}^{239}Pu^{16}O^+$; $^{238}U^1H^+ \rightarrow {}^{238}U^{16}O^+$, $^{238}U^{16}O_2{}^+$	128

reaction gas. The application of CO_2 or NH_3 permitted the measurement of radionuclides of Pu in on-mass mode, with interfering ions transferred to related polyatomic ions.

5 Protocols for post-analysis mathematical correction

Taking advantage of the capability of ICP-QMS/QMS for spectral separation, interferences from oxide ions of LREEs and MREEs in the measurement of MREEs and HREEs, respectively, can be effectively separated using the appropriate reaction gases. It is notable that the interferences from oxide ions and hydroxide ions of Ba with the measurement of Eu can be substantial for natural samples, which is attributed to the much higher (by over 3 orders of magnitude) concentration of Ba than that of Eu. The use of N_2O as the reaction gas helped convert Ba-related ions to higher-order (with multiple oxygen and hydrogen atoms) ions and resulted in much better separation from the signals for Eu isotopes.[33] When oxygen is used as the reaction gas, the interferences from Ba-related ions in the measurement of Eu isotopes may be still significant, which can be mathematically corrected based on the intensities of Ba-related ions observed in a Ba standard solution (interference factor, $\mathrm{InF} = S_{\mathrm{Eu}*}/S_{\mathrm{Ba}*}$; $S_{\mathrm{Eu}*}$ and $S_{\mathrm{Ba}*}$, signal intensities of Eu-seeming and Ba, respectively) and the concentrations of Ba in the samples ($S_{\mathrm{Eu}} = S_{\mathrm{Eu0}} - S_{\mathrm{Ba}} \times \mathrm{InF}$; S_{Eu}, S_{Eu0}, and S_{Ba}, signal intensities of Eu after correction, Eu before correction, and Ba, respectively). Based on the difference in the isotopic abundance of Ba-related interferences and that of Eu, Zhu and Itoh reported a pseudo-isotope dilution method for the correction of spectral interferences from Ba-related ions with the measurement of Eu.[158] In this method, the Ba-related interference was considered an analog of the ^{153}Eu-enriched isotope spike. As a result, the concentration of Eu in a sample can be calculated (based on the well-known isotope dilution equations) according to the ratio of ^{151}Eu/^{153}Eu in an Eu standard solution, Ba standard solution, and the sample. Due to the fact that the m/z value is dependent on ion transmission in the ICP-QMS/QMS system, correction of mass discrimination should be considered for the measurement of the isotopic ratio. Ohno and Muramatsu reported that the measured ^{134}Cs/^{137}Cs ratios in the samples by ICP-QMS/QMS were consistent with the values determined by Ge semiconductor analysis within the analytical error, even without any correction of the mass-discrimination effect.[48] This can be attributed to the fact that the practical relative analytical errors were in the range of 15% to 28%, which is higher than the extent of mass-discrimination in the measurement by ICP-QMS/QMS. When a result is required with a smaller relative analytical error (*e.g.* less than 5%), mass-discrimination can be critical. Zok *et al.* corrected the mass bias of the plasma with an external europium reference solution (5 ppb) spiked to a blank-processed eluate to achieve a comparable matrix as that of the samples for ^{135}Cs/^{137}Cs ratio measurement.[101] Due to the lack of a ^{135}Cs/^{137}Cs certified solution, Magre *et al.* corrected the mass bias using the sample-standard bracketing approach with a solution previously qualified by TIMS.[120] Ohno *et al.* reported the correction of ^{127}I-related interference in the measurement of ^{129}I based on the observed ratio of ^{127}I(H$_2$ and D)$^+$/^{127}I$^+$ in a natural iodine standard solution. Lindahl *et al.* reported the precise measurement of the ^{233}U/^{235}U ratio with a relative standard deviation of 0.07% after linear mode correction of mass-discrimination (*i.e.* mass bias).[88] To achieve the ultra-trace-level measurement of the ^{240}Pu/^{239}Pu ratio, Zheng and Yamada corrected the mass bias with a Pu isotope certified standard solution (NBS-947).[159]

Dead time correction should be considered when measuring isotopic ratios with high signal intensities in pulse mode.[160] The effect of dead time is more prominent for larger isotopic ratios, *e.g.* over 10^6 or under 10^{-6} requiring measurements with signal intensities over one million counts per second (CPS). A simple model for dead time correction is as follows: $I_1 = I_0/(1 - I_0 \times t)$, where I_1, I_0, and t are the true signal intensity, observed intensity, and deadtime, respectively.

6 Selected applications and representative analytical figures of merits

6.1 Selected applications for the measurement of REEs

Galusha *et al.* reported a method for quantifying REEs in digested bone samples, with O_2 reaction for Tb and Lu, while using H_2 reaction for other REEs.[18] The method detection limits for REEs ranged from 0.9 ng per g (Tm) to 5.6 ng per g (Nd). The median values of REEs in the parental nutrition patient group were at least fifteen times higher than that of the "control" group and exceeded all previously reported data.

Ding *et al.* developed a simple and reliable chemical procedure for the separation of REEs from a uranium matrix before measurement by ICP-QMS/QMS.[23] REEs were measured in mass-shift mode by using O_2 as the reaction gas, which helped the effective suppression of polyatomic interferents in the measurement of REEs. The method detection limits for all REEs were below 1 pg mL^{-1}, which ensured the precise and accurate measurement of REEs in small amounts of uranium ore samples.

Zhu compared N_2O and O_2 as the reaction gases for the measurement of REEs in mass-shift mode.[33] The results showed that the N_2O reaction apparently improved the yields of ^{m}M^{16}O$^+$ for Eu and Yb, which helped improve the sensitivities for the measurement of Eu and Yb in comparison to that obtained with O_2 as the reaction gas. A typical sensitivity of 300 000 CPS per ng per mL was obtained for REEs measured with an isotope having an isotopic abundance close to 100%. Furthermore, the N_2O reaction also helped suppress Ba-related spectral interferences in the measurement of Eu and permitted the measurement of Eu in natural samples without mathematic correction of the spectral interferences. The instrumental detection limits for REEs ranged from 0.004 pg mL^{-1} of Tm to 0.028 pg mL^{-1} of La.

A comparison of the representative detection limits and sensitivities for the measurement of REEs is summarized in Table 7. It is notable that the method detection limit (MDL) cannot be simply compared due to their dependence on the pretreatment procedures. The sensitivities can be compared because they are all given as the signal intensities corresponding to 1.0 ng mL^{-1} of each REE. It can be seen that the

Table 7 Comparison of the detection limits and sensitivities obtained for the measurement of REEs[a]

		Galusha *et al.*[18] (H_2, O_2 reaction)		Ding *et al.*[23] (O_2 reaction)		Zhu[33] (O_2 reaction)		Zhu[33] (N_2O reaction)	
Element	*m*/*z*	MDL[b] (ng g^{-1})	Sensitivity[c]	MDL[b] (pg mL^{-1})	Sensitivity[c]	IDL[d] (pg mL^{-1})	Sensitivity[c]	IDL[d] (pg mL^{-1})	Sensitivity[c]
La	139	5.1	10 538	*0.52*	*290 000*	*0.030*	*220 985*	*0.028*	*254 917*
Ce	140	4.7	90 978	*0.63*	*170 000*	*0.024*	*217 929*	*0.018*	*238 483*
Pr	141	1.6	158 370	*0.16*	*350 000*	*0.017*	*285 257*	*0.006*	*327 937*
Nd	146	5.6	16 258	*0.69*	*61 000*	*0.022*	*48 482*	*0.026*	*59 753*
Sm	147	3.7	22 343	*0.28*	*52 000*	*0.043*	*37 733*	*0.006*	*52 160*
Eu[e]	151(i), 153(ii)	1.0(i)	41 925(i)	*0.98(ii)*	*39 000(ii)*	*0.024(ii)*	*44 838(ii)*	*0.010(ii)*	*196 360(ii)*
Gd	157	5.3	23 049	*0.50*	*52 000*	*0.011*	*39 670*	*0.017*	*52 342*
Tb	159	*1.1*	*35 264*	*0.10*	*340 000*	*0.007*	*261 392*	*0.006*	*331 227*
Dy	163	2.8	22 441	*0.15*	*90 000*	*0.033*	*66 508*	*0.016*	*86 904*
Ho	165	2.7	90 794	*0.11*	*350 000*	*0.010*	*260 269*	*0.010*	*324 374*
Er	166	1.3	46 782	*0.20*	*120 000*	*0.020*	*81 849*	*0.016*	*106 869*
Tm	169	0.9	96 712	*0.17*	*310 000*	*0.012*	*224 416*	*0.004*	*320 798*
Yb[e]	172(i), 174(ii)	1.3(ii)	30 894(ii)	*0.77(i)*	*13 000(i)*	*0.060(i)*	*18 069(i)*	*0.023(i)*	*62 655(i)*
Lu	175	*1.6*	*31 402*	*0.15*	*330 000*	*0.019*	*233 119*	*0.012*	*312 566*

[a] Italic data were obtained *via* mass-shift mode (*e.g.* $^{139}La^+ \rightarrow {}^{139}La^{16}O^+$) measurements. [b] MDL, method detection limit. [c] Sensitivity unit, CPS per ng mL^{-1}. [d] IDL, instrumental detection limit. [e] (i) and (ii) Different choices of isotopes for measurement.

measurements conducted in mass-shift mode (italic data) provided higher sensitivities in comparison to that obtained in on-mass mode. These results can be attributed to the difference in operating conditions, where in the case of on-mass mode measurement, a neutral or positive energy discrimination was applied at the under stream of the CRC, resulting in a decrease in the transmission of positively charged ions to the second quadrupole mass filter. By contrast, negative energy discrimination was applied for mass-shift mode and was beneficial for the improvement in the transmission of positively charged ions to the second quadrupole mass filter.

It is noteworthy that the sensitivities for Eu and Yb were relatively lower when measured in mass-shift mode with oxygen as the reaction gas, which was attributed to the exothermic reactions for producing MO^+ from M^+. The introduction of N_2O as the reaction gas helped overcome this problem and provided the best performance for measuring the whole set of REEs.

6.2 Selected applications for the measurement of radioactive Cs

Cao *et al.* developed an analytical method for the simultaneous determination of radioactive Cs and Pu isotopes in suspended particles with a small sample size (1–2 g), which was applied to suspended particles of river water samples collected from the Fukushima Prefecture after the Fukushima Daiichi Nuclear Power Plant (FDNPP) accident.[52] The $^{135}Cs/^{137}Cs$ atom ratios (0.329–0.391) and ^{137}Cs activities (23.4–152 Bq g^{-1}) suggested that the radioactive Cs contamination in the suspended particles mainly originated from the accident-released radioactive contaminates. In addition, most of the detected radioactive Cs at northwest of the FDNPP site was likely to be derived from a mixture of reactor Units 2 and 3, given that the observed $^{135}Cs/^{137}Cs$ atom ratios (0.333–0.355) in the environmental samples collected northwest from the FDNPP site appeared to be consistent with reactor Units 2 (0.341) and 3 (0.350). The Pu contamination in the suspended particles caused by the accident could be neglected given that the $^{240}Pu/^{239}Pu$ atom ratios (0.182–0.208) were in the range of global fallout.

Zheng *et al.* developed a method to accomplish the sufficient separation of major elements (such as Ca, K, and Mg) for measuring trace radioactive Cs in large volume samples.[57] The separation was achieved using a 2 mL AG MP-1M resin column, 10.5 mL AG 50W-X8 resin packed in an Eppendorf pipette, and 2 mL Sr resin cartridge, resulting in the complete removal of the interfering elements in large-size samples (up to 40 g soil and sediment samples) for the analysis of low-level ^{137}Cs (20–1000 Bq kg^{-1}). This separation method showed high decontamination factors (10^4–10^7) for major matrix elements (Al, Ca, K, Mg, Na and Si) and interfering elements (10^5–10^6 for Ba, 10^6–10^7 for Mo, 10^4–10^6 for Sb and 10^4–10^5 for Sn) for 10–40 g soil and sediment samples. By using an Apex-Q sample introduction system, the measurement sensitivity was significantly improved to 2.95×10^5 cps for 1 ng per mL ^{133}Cs standard solution. Seven reference materials were used for the method validation. The JSAC-0471 (soil), JSAC-0766 (soybean) and JSAC-0776 (mushroom) reference materials collected 100–250 km southwest of the FDNPP site within the Kanto region of Japan following the Fukushima accident presented the $^{135}Cs/^{137}Cs$ isotope ratios of 0.378 ± 0.023, 0.353 ± 0.025, and 0.378 ± 0.021, respectively (decay corrected to March 11, 2011). In the case of IAEA-soil-6 (soil from the Upper Austria before the Chernobyl accident), with low ^{137}Cs activity of 28.1 Bq kg^{-1}, the $^{135}Cs/^{137}Cs$ ratio was measured to be 2.58 ± 0.37 (decay corrected to January 1, 2015). In the case of IAEA-385 (marine sediment from the Irish Sea), with the lowest ^{137}Cs activity of 23.3 Bq kg, the $^{135}Cs/^{137}Cs$ ratio was measured to be 1.21 ± 0.14 (decay corrected to January 1, 2015). For IAEA-330 (Spinach) and IAEA-156 (Clover) (contaminated by radioactive Cs due to the Chernobyl accident), the $^{135}Cs/^{137}Cs$ ratio was measured to be 0.546 ± 0.031, and 0.541 ± 0.027, respectively (decay corrected to January 1, 2015). Using this ICP-QMS/QMS analytical method, Stäger *et al.* investigated

radiocesium contamination in wild boars from Bavaria.[139] Chornobyl has been widely believed to be the prime source of ^{137}Cs in wild boars; however, using the emerging nuclear forensic fingerprint, ^{135}Cs/^{137}Cs ratio, they found that "old" ^{137}Cs from global fallout significantly contributed to the total level (10–68%) in the investigated specimens that exceeded the regulatory limit (600 Bq kg^{-1}).

Zhu *et al.* compared acid leaching using aqua regia and alkali fusion using $LiBO_2$ for the recovery of radioactive Cs from large-size soil samples (1–60 g).[84] Alkali fusion resulted in high recovery of >93% due to the complete decomposition, while acid leaching presented a high leaching efficiency (>85% for samples less than 10 g and even >60% for samples up to 60 g). Given that acid leaching is simple, with easy operation, less time-consuming, and more suitable for the treatment of large-size samples compared with the fusion method, acid leaching using aqua regia with a sample/acid ratio of 1 : 8 at 180 °C for 2 h was recommended and used. After preconcentration by AMP-PAN, NH_4HCO_3, $(NH_4)_2CO_3$, NH_4F, $NH_4C_2O_4$, NH_4Ac, and NH_4Citr solution could directly dissolve the AMP component, similar to ammonia solution. Considering the easy removal of NH_4Cl by the heating method based on its sublimation at low temperatures (338 °C), the risk for dangerous explosion of NH_4NO_3 during heating, and difficulties in the removal of sulfate, NH_4Cl was selected to elute Cs^+ from the AMP-PAN resin. Based on the low sublimation temperature of NH_4Cl (338 °C) but not CsCl, a simple heating method was developed to remove NH_4Cl by sublimation. The increased recoveries of Cs from 31% to 99% with the amount of LiCl of 60 mg confirmed that a sufficient amount of particles/salt is important for preventing the loss of Cs during the sublimation of NH_4Cl. A 10 mL cation exchange resin (AG50W-X8) in a column of $\varphi 1.0 \times 20$ cm was employed for achieving the better separation of Cs from Ba, Rb, and K. The overall decontamination factors of 4×10^7 for Ba, 4×10^6 for Li, 4×10^5 for Mo, 3×10^5 for Sn, and 2×10^5 for Sb were achieved. Also, the high throughput of 8 samples per 3 days was achieved. The measured ^{135}Cs/^{137}Cs atomic ratios (decay corrected to 1st Feb 2020) in soils collected from Gavle, Sweden and Feofaniya, Ukraine were similar (0.65–0.71), although the ^{137}Cs concentrations (140–1650 Bq kg^{-1}) were significantly different. This indicated that most of the radioactive Cs in these samples originated from the Chernobyl accident fallout. Much higher ^{135}Cs/^{137}Cs atomic ratios (2.08–2.68, decay corrected to 1st Feb 2020), but much lower ^{137}Cs concentrations (3–8 Bq kg^{-1}) were observed in soil samples from Denmark. By calculation, the contributions of radioactive Cs from the Chernobyl accident were estimated to be 31% and 51% for these two soil samples, respectively.

6.3 Selected applications for the measurement of radioactive Sr

Amr *et al.* investigated ICP-QMS/QMS as a practical, fast, and reliable method for the ultra-trace determination of anthropogenic radionuclides including ^{90}Sr, ^{137}Cs, ^{238}Pu, ^{239}Pu, and ^{240}Pu, considering the accuracy and precision for producing reliable results.[51] The radionuclides were extracted from 1 kg of environmental soil samples using concentrated nitric and hydrochloric acid. The concentrations of ^{90}Sr, ^{137}Cs, ^{238}Pu, ^{239}Pu, and ^{240}Pu in certified reference materials (NIST SRM 4354, IAEA-375) were measured for validation. The developed methods were applied to measure the anthropogenic radionuclides in soil samples collected throughout the State of Qatar. The average concentrations of ^{90}Sr, ^{137}Cs, ^{238}Pu, ^{239}Pu, and ^{240}Pu were 0.606 fg g^{-1} (3.364 Bq kg^{-1}), 0.619 fg g^{-1} (2.038 Bq kg^{-1}), 0.034 fg g^{-1} (0.0195 Bq kg^{-1}), 65.59 fg g^{-1} (0.150 Bq kg^{-1}), and 12.06 fg g^{-1} (0.103 Bq kg^{-1}), respectively.

Tomita *et al.* developed a rapid analytical method for determining ^{90}Sr in urine samples (1–2 L) to assess the internal exposure of workers in a radiological emergency.[72] Strontium in a urine sample was rapidly separated by phosphate co-precipitation, followed by extraction chromatography, and the ^{90}Sr activity was determined by ICP-QMS/QMS. Measurement in on-mass mode with an O_2 reaction gas flow rate of 1 mL min^{-1} showed no tailing of ^{88}Sr at $m/z = 90$ up to 50 mg per L Sr. The interferences of Ge, Se and Zr at $m/z = 90$ were successfully removed by phosphate co-precipitation, followed by extraction chromatography with a tandem column of Pre-filter, Eichrom TRU and Sr resin. This analytical method was validated by the results of the analyses of synthetic urine samples (1.2–1.6 L) containing a known amount of ^{90}Sr together with 1 mg of each of Ge, Se, Sr and Zr. The turnaround time for Sr purification from the urine sample to ^{90}Sr measurement was about 10 h. The detection limit of ^{90}Sr was approximately 1 Bq per urine sample, which was lower than 15 Bq per urine after a day of intake, giving 5 mSv of unplanned exposure of worker limited by the Nuclear Regulation Authority of Japan.

Wang *et al.* developed an online separation and preconcentration method employing a lab-on-valve system for the analysis of ^{90}Sr in various water/wastewater samples.[93] ^{90}Sr was separated from ^{90}Zr, an isobaric interference present at high concentrations in many samples, and other matrix components using a dual-column setup (Eichrom DGA-Branched resin and Sr resins). Subsequently, any remaining ^{90}Zr was chemically resolved from the ^{90}Sr in the measurement by ICP-QMS/QMS using O_2 and H_2 as the reaction gases. This system required small sample volumes (10 mL), minimal sample preparation compared to traditional radiometric, and other ICP-MS techniques and has a processing time of 22 min per sample. Based on a 10 mL sample size, the system limit of detection, limit of quantification and method detection limit (MDL) were 0.47 Bq L^{-1} (0.09 pg L^{-1}), 1.57 Bq L^{-1} (0.32 pg L^{-1}) and 1.79 Bq L^{-1} (0.34 pg L^{-1}), respectively. Recovery of the IAEA 2018 Proficiency Test Exercise water sample ($n = 5$) was 99% with an RSD of 11.9%. Thus, this method provides a powerful tool for the rapid analysis of low levels of ^{90}Sr.

Suzuki *et al.* developed a new analytical system that enables the real-time analysis of ^{90}Sr in atmospheric particulate matter with an analytical run time of only 10 min.[59] After passage of an air sample through an impactor, a small fraction of the sample is introduced into a gas-exchange device, where the air is replaced by Ar. Then, the sample is directly introduced into the ICP-QMS/QMS for measurement, where the separation of isobaric interferences on $^{90}Sr^+$ from $^{90}Zr^+$, $^{89}Y^1H^+$, and $^{90}Y^+$ was

investigated under various reaction gas conditions. The results showed that interferences could be minimized under the optimized conditions of 1 mL per min O_2, 10 mL per min H_2, and 1 mL per min NH_3. The estimated background equivalent concentration and estimated detection limit of the system were 9.7×10^{-4} and 3.6×10^{-4} ng m^{-3}, which are equivalent to 4.9×10^{-6} and 1.8×10^{-6} Bq cm^{-3}, respectively. The recoveries of Sr in $PM_{2.5}$ measured by real-time analysis compared to that obtained by simultaneously collection on the filter was 53% ± 23%, and using this recovery, the detection limit of $PM_{2.5}$ was estimated to be $3.4 \pm 1.5 \times 10^{-6}$ Bq cm^{-3}. Specifically, this system enabled the detection of ^{90}Sr at concentrations of $<5 \times 10^{-6}$ Bq cm^{-3}, even considering the insufficient fusion/vaporization/ionization efficiency of Sr in $PM_{2.5}$.

For ^{90}Sr analysis, the application of O_2 as the reaction gas to mitigate isobaric and polyatomic interferences (*e.g.* $^{90}Zr^+$ and $^{89}YH^+$) resulted in serious polyatomic interferences due to oxides (*e.g.* $^{72}Ge^{18}O^+$ and $^{74}Ge^{16}O^+$). Yang *et al.* developed a rapid ^{90}Sr bioassay in small-amount urine (10–400 mL) using ICP-QMS/QMS, with the introduction of the innovative reaction gas of CO_2.[137] After organic matter decomposition and chemical separation, stacked DGA and Sr resin cartridges were used directly for the chromatographic separation and purification of Sr. The Sr yields were measured to be 94% ± 5% (n = 12) for the whole procedure, using stable ^{88}Sr originally in the urine sample as a yield tracer. The produced ions in the CRC demonstrated that oxygen transfer and CO_2 clusterization occur after the reaction between CO_2 and Zr, further mitigating the isobaric interference from ^{90}Zr, compared to the O_2 reaction gas. The false signal intensities resulting from $^{72}Ge^{18}O^+$ and $^{74}Ge^{16}O^+$ using CO_2 reaction gas also deceased to about 1/5 of that using O_2 reaction gas. For further method validation, the ^{90}Sr concentrations in urine samples were measured during the PROCORAD (Association for the PROmotion of Quality COntrol in RADiotoxicological Analysis) intercomparison campaign. All the results were in good agreement with the assigned values.

6.4 Selected applications for the measurement of radioactive I

Shikamori *et al.* reported the first measurement of ^{129}I by ICP-QMS/QMS with O_2 as the reaction gas.[46] The IDL and the BEC values observed by on-mass measurements of ^{129}I in various concentrations of NIST SRM 3231 Level I were 0.07 pg mL^{-1} and 0.04 pg mL^{-1}, respectively.

Coralie *et al.* reported the first mass-shift measurement of ^{129}I by ICP-QMS/QMS with O_2 as the reaction gas.[138] Measurements with N_2O and CO_2 as the reaction gases were also performed but showed lower sensitivity than that obtained with O_2 reaction. Multiple surfactants were investigated as reagents to improve the sensitivity for measuring iodine. A signal gain of 2.5 was achieved by adding 3% surfactant, while this gain was independent of the type of surfactant. The optimal measurement medium for the measurement of iodine was a solution of 0.1% NH_4OH (v/v), 3% Tween 20, and 10 g per L ascorbic acid, achieving the IDL and BEC values of 1.7 pg mL^{-1} and 2.9 pg mL^{-1}, respectively. A ratio of 3.8×10^{-9} was achieved for the analysis of $^{129}I/^{127}I$.

Ohno *et al.* developed a new method for the determination of ^{129}I in soil samples using ICP-QMS/QMS with O_2 as the reaction gas and on-mass measurement with the objective of investigating radioiodine released by the FDNPP accident.[135] By measuring the $^{129}I/^{127}I$ ratio in NIST SRM 3231 Level II standard solution, they demonstrated the reliability of the developed ICP-QMS/QMS method for the measurement of the $^{129}I/^{127}I$ ratios at a level of 10^{-8}–10^{-9}.

Zhu and Asakawa reported the mass-shift measurement of ^{129}I by ICP-QMS/QMS with on-line generated ozone (*ca.* 10.5% O_3 in O_2) as the reaction gas.[141] Due to the exothermic reactions, the yields of oxide and dioxide ions of iodine were significantly improved by ozone reaction in comparison to that obtained by oxygen reaction. Using H_2 as an additional reaction gas helped reduce the residual spectral interference of $^{129}Xe^{16}O^+$ with the measurement of $^{129}I^+ \rightarrow {}^{129}I^{16}O^+$, achieving the IDL and the BEC values of 0.062 pg mL^{-1} and 0.016 pg mL^{-1}, respectively. The best analytical performance for $^{129}I/^{127}I$ ratio analysis was achieved by measuring $(^{129}I^+ \rightarrow {}^{129}I^{16}O_2^+)/(^{127}I^+ \rightarrow {}^{127}I^{16}O_2^+)$, resulting in a ratio of 6.7×10^{-10} in 500 μg per mL natural iodine solution.

6.5 Selected applications for the measurement of U isotopes

Tanimizu *et al.* attempted to measure the $^{236}U/^{238}U$ atom ratios at the environmental level by taking advantage of ICP-QMS/QMS for ^{236}U ($^{236}U/^{238}U$ atom ratio) measurements, the demand of which is increasing in various fields.[47] The following approaches were investigated to reduce ^{235}U and ^{238}U tailing and ^{235}U hydride interference: a desolvation system (ARIDUS) was employed, which is effective in improving the sensitivity and reducing hydrides; and uranium was measured as a monoxide by introducing O_2 as the reaction gas. Mass fractionation of $^{236}U/^{238}U$ was corrected using the SRM of Tl isotopes (mass numbers 203 and 205). As a result, the $^{236}U/^{238}U$ atom ratio could be measured in the range of 10^{-9} to 10^{-7}.

Jaegler and Gourgiotis measured U isotope ions as their dioxides by introducing N_2O as the reaction gas while using a desolvation system (APEX Ω) for sample introduction.[117] As a result, tailing from the major isotopes and hydride interference were significantly reduced and the $^{236}U/^{238}U$ isotope ratio at the 10^{-11} level could be precisely measured. This method has potential applications in various geochemical studies.

Lindahl *et al.* conducted a detailed study on the stability of ICP-QMS/QMS in measuring U concentrations and isotope ratios.[88] The results showed that the drift could reach up to 100%, which is probably due to the instability of the electronic components/devices associated with the quadrupole. Thus, to solve this problem, corrections were necessary for the accuracy and the precision by means of the appropriate adjustment of the mass resolution and the sample standard bracketing method. This worked showed that the instrumental stability also requires careful attention during the mass spectrometry determination of uranium isotopes.

6.6 Selected applications for the measurement of Pu isotopes

Bradley *et al.* integrated a microextraction sampling technique with ICP-QMS/QMS for the direct analysis of U and Pu from cotton swipes.[112] Once extracted, the sampled U/Pu were directed into the ICP-QMS/QMS, where CO_2 and He were introduced as the reaction gases for ion separation. By forming UO^+, U was ultimately separated from the Pu^+ ions of interest. This study demonstrated the direct liquid extraction of U and Pu from a cotton swipe solid surface and subsequent measurement of both U and Pu isotopes without chemical separation.

Huang *et al.* reported a rapid analytical method for the simultaneous determination of ^{238}Pu, ^{239}Pu, ^{240}Pu and ^{241}Pu using ICP-QMS/QMS after chemical separation.[116] A high decontamination factor of 2.19×10^9 for the most critical interfering element (*i.e.* U) was obtained with effective chemical separation using two sequential TK200 columns. The interferences of $^{238}U^1H^+$ and $^{238}U^+$ were effectively eliminated due to their conversion to UNH^+ and UNH_2^+, respectively, with NH_3 as the reaction gas for ICP-QMS/QMS. Given that Pu hardly reacts with NH_3 and remains as Pu^+, on-mass mode measurement was performed to realize the simultaneous determination of the hard-to-measure ^{238}Pu, ^{239}Pu, ^{240}Pu and ^{241}Pu in environmental samples at fg (*i.e.* 10^{-15} g) levels.

Zhang *et al.* developed a method using ICP-QMS/QMS measurement in mass-shift mode with O_2 and He as the reaction gases combined with a chemical separation procedure.[98] The reaction with O_2 gas converted Pu^+ to PuO_2^+, while polyatomic ions of Pb, Hg and Tl were difficult to react with O_2 to form new interfering ions at m/z 271 or 272. Thus, when Pu was measured in mass-shift mode at m/z 271 and 272 (PuO_2^+), the interferences from Pb, Hg and Tl were completely eliminated. In addition, the lower peak tailing of $^{238}U^+$ ($<5 \times 10^{-12}$) and the reduced $^{238}UO_2H^+/^{238}UO_2^+$ atomic ratio (4.82×10^{-9}) significantly suppressed the ^{238}U-derived interferences. Combined with a UTEVA chromatographic separation, the overall high elimination efficiency of U interferences up to 10^{14} could be achieved. Thus, the wide application of the developed method for the accurate determination of fg-level ^{239}Pu in high U samples, such as large-size deep seawater, deep layer soil and sediment, uranium debris of nuclear fuel, can be expected.

6.7 Merits of ICP-QMS/QMS for the measurement of radionuclides in comparison to multi-collector (MC-) ICP-MS

MC-ICP-MS is well-known for its capability to measure isotopic ratios at extremely high precision (*e.g.* relative standard deviation <0.01%) to differentiate samples with minute variations in isotopic ratio (*e.g.* <0.1%). However, the design of MC-ICP-MS for high-precision measurement has a trade-off of sensitivity, where a U solution of 10 ng mL^{-1} will be considered as a quite low-level.[161]

By contrast, radionuclides usually require measurement at lower pg mL^{-1} or even fg mL^{-1}, as stated in the above-selected applications. As a single detector instrument, ICP-QMS/QMS provides a typical relatively standard deviation of approximately 0.1% to 0.3% for isotopic ratio measurement at 1.0 ng per mL solution. This precision is sufficient for isotopic ratio measurement in radionuclides analysis, considering the large variation in isotopic ratio of over 10 or even 100-fold.

Because of its potential for effective spectral separation without sacrificing sensitivity, ICP-QMS/QMS provides an ideal approach for measuring radionuclides. An additional merit provided by ICP-QMS/QMS is its capability for the quasi-simultaneous screening of multi-radionuclides in the full m/z range (*e.g.* 2 to 260), while the m/z range measured simultaneously by MC-ICP-MS usually covers a narrower range (*e.g.* approximately 20).

7 Challenges and prospects for future research

Acid digestion or acid leaching is often used to transform solid samples to solutions, which may be subjected to further chemical separation prior to measurement by ICP-QMS/QMS.[78,84,96,110,113] Alkali fusion is also used for the complete dissolution of difficult-to-digest samples.[78,96,110] It is notable that fusion with ammonium bifluoride (ABF) has been shown to be an effective method to convert solid samples to solutions prior to elemental analysis.[162–168] It can be expected as an alternative to acid digestion/leaching and alkali fusion for the analysis of REEs and radionuclides.

The analysis of radionuclides in solid samples also involved complicated chemical separation with multiple solid phase columns.[49,52,57] Thus, it can expected that automation of these chemical separation process will be beneficial for the analysis of radionuclides by ICP-QMS/QMS.[11] The works by Ohira's group showed that the use of electrodialytic devices can be an effective approach for the separation and enrichment of trace elements prior to the measurement by an instrument.[169,170] This new type of technique may find application in the analysis of REEs and radionuclides by ICP-QMS/QMS in the near future.

The application of various reactive gases (H_2, O_2, NH_3, N_2O, CO_2, *etc.*) helped separate spectral interferences in the measurement of REEs and radionuclides. One of the most challenging works in the measurement of radionuclides is the analysis of ^{238}Pu in a uranium matrix, which contains a high concentration of ^{238}U. The application of He and NH_3 as the reaction gases resulted in a ratio of ^{239}Pu/^{238}U in the order of 10^{-9}.[116] However, a 1.0 ng per mL uranium solution will result in a signal intensity for ^{238}Pu equivalent to 0.2 pg per mL Pu. Further investigation of more effective methods for the separation of Pu and U is required for the direct measurement of a much lower Pu content in a higher concentration of U samples. Ozone has been shown to be effective for separating spectral interferences in the measurement of ^{129}I and may find more applications in the measurement of other RNs.

The Agilent 8800 and 8900 ICP-QMS/QMS have been mostly used in works on radionuclides to date. However, one of their limitations is their upper limit of m/z range for the second quadrupole, which is 260 and 275 for 8800 and 8900, respectively. This configuration limited the investigation of higher order cluster ions of actinides, *e.g.* the measurement of $^{238}U(^{14}N^1H_3)_3^+$, requiring a range of up to 289. Extension of this

limit to over 300 will be helpful for works on the measurement of actinides by ICP-QMS/QMS, providing sufficient investigation and application about the mechanism of related ion–molecule reactions.

8 Conclusions

ICP-QMS/QMS has been widely investigated and applied in the analysis of REEs and RNs in various research fields since its commercial availability in 2012. The Agilent 8800 and 8900 are mostly used in the works published to date, with the increasing application of iCAP TQ and NexION 5000 in recent years.

In addition to He, H_2, O_2, and NH_3, which are usually standard in the instruments, N_2O and CO_2 have also been widely used as reaction gases in measurement by ICP-QMS/QMS. The application of N_2O and CO_2 specially helped separate spectral interferences in measuring RNs of Cs, Sr, U, and Pu.

Acid digestion, acid leaching, and alkali fusion have often been used to convert solid samples to solutions, followed by chemical separation such as SPE, solvent extraction, and coprecipitation.

ICP-QMS/QMS has shown excellent performances for the analysis of REEs and RNs, which is attributed to the effectiveness of separating spectral interferences by using the well-controlled ion–molecule reactions in the reaction cell. Extension of the upper limit of the m/z range of the second quadrupole mass filter will be beneficial for further works on actinides.

Data availability

All the data are presented within the article.

Author contributions

Yanbei Zhu: conceptualization, methodology, writing – original draft preparation (general, I-129, and REEs related), supervision. Guosheng Yang: writing – original draft (Cs related). Aya Sakaguchi: writing – original draft (U related). Tsutomu Miura: writing – original draft (Sr related). Yasuyuki Shikamori: investigation, reviewing and editing. Jian Zheng: conceptualization, methodology, writing – original draft (Pu related), supervision.

Conflicts of interest

There are no conflicts to declare.

Acknowledgements

The present work was supported by grants from the Japan Society for the Promotion of Science: 18K19849 (Sakaguchi), 21H03609 (Sakaguchi), 22K05181 (Zhu), 24K01394 (Zhu and Shikamori), JP17K00537 (Zheng), and 22K12384 (Yang and Zheng). The support from the Managing Director's Fund of the Quantum Medical Science Directorate, QST (Zheng and Yang) and the ERAN project P-24-05 (Zheng and Sakaguchi) is also acknowledged.

Notes and references

1 N. Sugiyama and G. Woods, *Application Note*, Report 5991-0892JAJP, Agilent Technologies, 2013.
2 N. Yamada and J. Takahashi, *Bunseki Kagaku*, 2018, **67**, 249–279.
3 V. Balaram, *Minerals*, 2023, **13**, 1031.
4 S. Diez-Fernández, H. Isnard, A. Nonell, C. Bresson and F. Chartier, *J. Anal. At. Spectrom.*, 2020, **35**, 2793–2819.
5 V. Balaram, *Rapid Commun. Mass Spectrom.*, 2021, **35**, e9065.
6 W. T. Bu, J. Zheng, X. M. Liu, K. M. Long, S. Hu and S. Uchida, *Spectrochim. Acta B Atom Spectrosc.*, 2016, **119**, 65–75.
7 O. T. Butler, W. R. L. Cairns, J. M. Cook and C. M. Davidson, *J. Anal. At. Spectrom.*, 2015, **30**, 21–63.
8 O. T. Butler, W. R. L. Cairns, J. M. Cook, C. M. Davidson and R. Mertz-Kraus, *J. Anal. At. Spectrom.*, 2018, **33**, 8–56.
9 Q. Ma, Z. M. Yang, Y. H. Yang and Z. Y. Chu, *Ore Geol. Rev.*, 2023, **163**, 105764.
10 Y. B. Zhu, T. Ariga, K. Nakano and Y. Shikamori, *Atom. Spectrosc.*, 2021, **42**, 299–309.
11 Y. Y. Ni, Y. Liu, W. T. Bu, C. T. Yang and S. Hu, *TrAC, Trends Anal. Chem.*, 2023, **168**, 117329.
12 W. M. Wu, H. L. Liu and T. F. Zheng, *Chin. J. Anal. Chem.*, 2015, **43**, 697–702.
13 J. Song, X.-C. Zeng, D. Yan and W.-M. Wu, *Application Note*, Report 5991-5400JAJP, Agilent technology, 2015.
14 C. Labrecque, P. J. Lebed and D. Larivière, *J. Environ. Radioact.*, 2016, **155**, 15–22.
15 A. Santoro, V. Thoss, S. R. Guevara, D. Urgast, A. Raab, S. Mastrolitti and J. Feldmann, *Appl. Radiat. Isot.*, 2016, **107**, 323–329.
16 S. C. Wu, X. C. Zeng, X. F. Dai, Y. P. Hu, G. Li and C. J. Zheng, *Spectrochim. Acta B Atom Spectrosc.*, 2016, **123**, 129–133.
17 L. Whitty-Léveillé, K. Turgeon, C. Bazin and D. Larivière, *Anal. Chim. Acta*, 2017, **961**, 33–41.
18 A. L. Galusha, P. C. Kruger, L. J. Howard and P. J. Parsons, *J. Trace Elem. Med. Biol.*, 2018, **47**, 156–163.
19 X. M. Zhang, X. F. Zeng, L. B. Liu, X. L. Lan, J. Huang, H. X. Zeng, R. Li, K. Q. Luo, W. Wu, M. H. Zhou and S. J. Li, *Oncol. Lett.*, 2018, **15**, 4121–4128.
20 N. Korf, A. N. Lovik, R. Figi, C. Schreiner, C. Kuntz, P. M. Mählitz, M. Rösslein, P. Wäger and V. S. Rotter, *Waste Manage.*, 2019, **92**, 124–136.
21 Y. Zhang, Z. B. Pan, P. C. Jiao, J. Ju, T. He, T. C. Duan and H. Q. Cai, *Atom. Spectrosc.*, 2019, **40**, 167–172.
22 Y. B. Zhu, *Talanta*, 2020, **209**, 120536.
23 X. T. Ding, W. T. Bu, Y. Y. Ni, X. P. Shao, K. Xiong, C. T. Yang and S. Hu, *J. Anal. At. Spectrom.*, 2021, **36**, 2144–2152.
24 B. T. Manard, D. A. Bostick, S. C. Metzger, B. W. Ticknor, N. A. Zirakparvar, K. T. Rogers and C. R. Hexel, *Spectrochim. Acta B Atom Spectrosc.*, 2021, **179**, 11.
25 G. Olszewski, P. Lindahl, P. Frisk, M. Eriksson and H. B. L. Pettersson, *Talanta*, 2021, **229**, 5.

26 A. Simpson, S. Gilbert, R. Tamblyn, M. Hand, C. Spandler, J. Gillespie, A. Nixon and S. Glorie, *Chem. Geol.*, 2021, **577**, 120299.
27 Y. B. Zhu, K. Nakano, Y. Shikamori and A. Itoh, *Spectrochim. Acta B Atom Spectrosc.*, 2021, **179**, 106100.
28 J. Gillespie, C. L. Kirkland, P. D. Kinny, A. Simpson, S. Glorie and K. Rankenburg, *Geochim. Cosmochim. Acta*, 2022, **338**, 121–135.
29 O. Klein, T. Zimmermann, L. Hildebrandt and D. Pröfrock, *Sci. Total Environ.*, 2022, **852**, 158464.
30 K. L. LeBlanc, K. Nadeau, J. Meija, L. Yang, P. A. Babay, M. A. Bavio, C. Boome, D. Chipley, R. S. C. Leguizamón, J. Denton, D. L. Drew, M. A. Fernández, V. Fugaru, V. D. Genetti, F. Gonzalez, J. D. Inglis, S. Jovanovic, E. Keegan, T. Kell, Y. Kimura, W. Kinman, S. Kiser, R. E. Lindvall, E. Loi, K. Mayer, J. F. Mercier, R. Millar, A. Nicholl, L. Orlovskaya, J. L. Ramella, A. Serban, M. A. Sharp, Y. Q. Shi, C. Tóbi, L. Valenzuela, Z. Varga, A. Vesterlund, M. Virgolici, H. Yamazaki, E. N. Zubillaga, A. El-Jaby and Z. Mester, *J. Radioanal. Nucl. Chem.*, 2022, **331**, 4031–4045.
31 T. Miura and A. Wada, *Front. Chem.*, 2022, **10**, 888636.
32 D. Subarkah, M. L. Blades, A. S. Collins, J. Farkas, S. Gilbert, S. C. Löhr, A. Redaa, E. Cassidy and T. Zack, *Geology*, 2022, **50**, 66–70.
33 Y. B. Zhu, *Front. Chem.*, 2022, **10**, 912938.
34 S. Glorie, J. Mulder, M. Hand, A. Fabris, A. Simpson and S. Gilbert, *Geosci. Front.*, 2023, **14**, 101629.
35 M. L. Harsha, E. A. Whisenhant, D. Hebert, J. Y. Do, C. Pham, P. Zito, D. C. Podgorski and P. L. Tomco, *Environ. Sci. Technol. Lett.*, 2023, **10**, 747–754.
36 A. Naccarato, M. L. Vommaro, D. Amico, F. Sprovieri, N. Pirrone, A. Tagarelli and A. Giglio, *Toxics*, 2023, **11**, 499.
37 C. Telloli, S. Tagliavini, F. Passarini, S. Salvi and A. Rizzo, *Food Chem.*, 2023, **402**, 134247.
38 L. W. Yang, T. Yang, J. T. Li, Y. B. Lin and H. F. Ling, *Ore Geol. Rev.*, 2023, **158**, 105480.
39 H. Y. Zhang, B. Fu, J. Wang, X. L. Ma, G. Q. Luo and H. Yao, *Spectrosc. Spectr. Anal.*, 2023, **43**, 2074–2081.
40 Z. Aktar and K. Toyoda, *Environ. Sci. Technol. Lett.*, 2024, **11**, 598–603.
41 F. Gaidies, T. McCarron, A. D. Simpson, R. M. Easton, S. Glorie, B. Putlitz and K. Trebus, *J. Metamorph. Geol.*, 2024, **42**, 35–61.
42 S. C. Löhr, C. Spandler and A. Baldermann, *Geochim. Cosmochim. Acta*, 2024, **366**, 48–64.
43 D. Wippermann, A. Zonderman, T. Zimmermann and D. Pröfrock, *Anal. Bioanal. Chem.*, 2024, **416**, 2797–2807.
44 V. K. Zepeda, B. S. Kamber and O. Y. A. Ghidan, *Chem. Geol.*, 2024, **647**, 121827.
45 S. H. Al-Meer, M. A. Amr, A. I. Helal and A. T. Al-Kinani, *Radioact. Waste Manage.*, 2013, **2**, 96160.
46 Y. Shikamori, K. Nakano, N. Sugiyama and S. Kakuda, *Application Note*, Report 5991-0321JAJP, Agilent Technologies, 2013.
47 M. Tanimizu, N. Sugiyama, E. Ponzevera and G. Bayon, *J. Anal. At. Spectrom.*, 2013, **28**, 1372–1376.
48 T. Ohno and Y. Muramatsu, *J. Anal. At. Spectrom.*, 2014, **29**, 347–351.
49 J. Zheng, W. T. Bu, K. Tagami, Y. Shikamori, K. Nakano, S. Uchida and N. Ishii, *Anal. Chem.*, 2014, **86**, 7103–7110.
50 R. S. Pappas, N. Martone, N. Gonzalez-Jimenez, M. R. Fresquez and C. H. Watson, *J. Anal. Toxicol.*, 2015, **39**, 347–352.
51 M. A. Amr, A. F. I. Helal, A. T. Al-Kinani and P. Balakrishnan, *J. Environ. Radioact.*, 2016, **153**, 73–87.
52 L. G. Cao, J. Zheng, H. Tsukada, S. M. Pan, Z. T. Wang, K. Tagami and S. Uchida, *Talanta*, 2016, **159**, 55–63.
53 N. Sugiyama, *Application Note*, Report 5991-6553JAJP, Agilent Technologies, 2016.
54 G. S. Yang, H. Tazoe and M. Yamada, *Anal. Chim. Acta*, 2016, **944**, 44–50.
55 G. S. Yang, H. Tazoe and M. Yamada, *Sci. Rep.*, 2016, **6**, 8.
56 G. S. Yang, H. Tazoe and M. Yamada, *Anal. Chim. Acta*, 2016, **908**, 177–184.
57 J. Zheng, L. G. Cao, K. Tagami and S. Uchida, *Anal. Chem.*, 2016, **88**, 8772–8779.
58 B. Russell, M. García-Miranda and P. Ivanov, *Appl. Radiat. Isot.*, 2017, **126**, 35–39.
59 Y. Suzuki, R. Ohara and K. Matsunaga, *Spectrochim. Acta B Atom Spectrosc.*, 2017, **135**, 82–90.
60 E. M. van Es, B. C. Russell, P. Ivanov and D. Read, *Appl. Radiat. Isot.*, 2017, **126**, 31–34.
61 G. S. Yang, H. Tazoe, K. Hayano, K. Okayama and M. Yamada, *Sci. Rep.*, 2017, **7**, 8.
62 L. Fu, S. Y. Shi, Y. G. Tang and H. Y. Wang, *Spectrosc. Spectr. Anal.*, 2018, **38**, 2588–2594.
63 T. Lu, X. L. Hou, L. Y. Zhang, N. Chen, W. C. Zhang and Y. Y. Wang, *Chin. J. Anal. Chem.*, 2018, **46**, 1137–1144.
64 J. X. Qiao and Y. H. Xu, *Talanta*, 2018, **183**, 18–23.
65 T. Suzuki, T. Yamamura, C. Abe, K. Konashi and Y. Shikamori, *J. Radioanal. Nucl. Chem.*, 2018, **318**, 221–225.
66 S. Xing, W. C. Zhang, J. X. Qiao and X. L. Hou, *Talanta*, 2018, **187**, 357–364.
67 E. Braysher, B. Russell, S. Woods, M. Garcia-Miranda, P. Ivanov, B. Bouchard and D. Read, *J. Radioanal. Nucl. Chem.*, 2019, **321**, 183.
68 X. L. Hou, W. C. Zhang and Y. Y. Wang, *Anal. Chem.*, 2019, **91**, 11553–11561.
69 H. Jaegler, F. Pointurier, S. Diez-Fernández, A. Gourgiotis, H. Isnard, S. Hayashi, H. Tsuji, Y. Onda, A. Hubert, J. P. Laceby and O. Evrard, *Chemosphere*, 2019, **225**, 849–858.
70 Y. Shao, G. S. Yang, D. D. Xu, M. Yamada, H. Tazoe, M. Luo, H. X. Cheng, K. Yang and L. L. Ma, *J. Environ. Radioact.*, 2019, **197**, 1–8.
71 L. Y. D. Tiong and S. M. Tan, *J. Radioanal. Nucl. Chem.*, 2019, **322**, 399–406.
72 J. Tomita and E. Takeuchi, *Appl. Radiat. Isot.*, 2019, **150**, 103–109.
73 P. E. Warwick, B. C. Russell, I. W. Croudace and Z. Zacharauskas, *J. Anal. At. Spectrom.*, 2019, **34**, 1810–1821.
74 S. Xing, M. Y. Luo, Y. Wu, D. Q. Liu and X. X. Dai, *J. Anal. At. Spectrom.*, 2019, **34**, 2027–2034.

75 G. S. Yang, J. Hu, H. Tsukada, H. Tazoe, Y. Shao and M. Yamada, *Environ. Pollut.*, 2019, **250**, 578–585.
76 G. S. Yang, M. S. Rahman, H. Tazoe, J. Hu, Y. Shao and M. Yamada, *Chemosphere*, 2019, **225**, 388–394.
77 W. C. Zhang, S. Xing and X. L. Hou, *Soil Tillage Res.*, 2019, **191**, 162–170.
78 C. Dalencourt, J. C. Tremblay-Cantin and D. Larivière, *J. Radioanal. Nucl. Chem.*, 2020, **326**, 1597–1607.
79 S. Diez-Fernández, H. Jaegler, C. Bresson, F. Chartier, O. Evrard, A. Hubert, A. Nonell, F. Pointurier and H. Isnard, *Talanta*, 2020, **206**, 8.
80 R. Q. Gao, X. L. Hou, L. Y. Zhang, W. C. Zhang and M. T. Zhang, *Chin. J. Anal. Chem.*, 2020, **48**, 765–773.
81 H. Jaegler, A. Gourgiotis, P. Steier, R. Golser, O. Diez and C. Cazala, *Anal. Chem.*, 2020, **92**, 7869–7876.
82 J. L. Mas, P. Aparicio, E. Galán, A. Romero-Baena, A. Miras, A. Yuste and D. Martín, *Appl. Clay Sci.*, 2020, **196**, 10.
83 T. Thabit, D. I. H. Elgeddawy and S. A. Shokr, *J. AOAC Int.*, 2020, **103**, 1282–1287.
84 L. C. Zhu, X. L. Hou and J. X. Qiao, *Anal. Chem.*, 2020, **92**, 7884–7892.
85 M. F. Alam, J. Hu, G. S. Yang, A. Ullah, M. I. Khalil, A. Kibria, I. M. M. Rahman, K. Nanba and M. Yamada, *J. Radioanal. Nucl. Chem.*, 2021, **330**, 103–111.
86 W. T. Bu, M. Gu, X. T. Ding, Y. Y. Ni, X. P. Shao, X. M. Liu, C. T. Yang and S. Hu, *J. Anal. At. Spectrom.*, 2021, **36**, 2330–2337.
87 A. L. Galusha, L. J. Howard, P. C. Kruger, T. Marks and P. J. Parsons, *J. Parenter. Enter. Nutr.*, 2021, **45**, 175–182.
88 P. Lindahl, G. Olszewski and M. Eriksson, *J. Anal. At. Spectrom.*, 2021, **36**, 2164–2172.
89 Y. Y. Ni, W. T. Bu, K. Xiong, X. T. Ding, H. Wang, X. M. Liu, K. M. Long and S. Hu, *Microchem. J.*, 2021, **169**, 6.
90 B. Russell, S. L. Goddard, H. Mohamud, O. Pearson, Y. Zhang, H. Thompkins and R. J. C. Brown, *J. Anal. At. Spectrom.*, 2021, **36**, 2704–2714.
91 B. Russell, H. Mohamud, M. G. Miranda, P. Ivanov, H. Thompkins, J. Scott, P. Keen and S. Goddard, *J. Anal. At. Spectrom.*, 2021, **36**, 845–855.
92 W. Wang, R. D. Evans and H. E. Evans, *Talanta*, 2021, **233**, 10.
93 W. Wang, R. D. Evans, K. Newman and R. Khokhar, *Talanta*, 2021, **222**, 8.
94 Y. Y. Wang, X. L. Hou, W. C. Zhang, L. Y. Zhang and Y. K. Fan, *Talanta*, 2021, **224**, 10.
95 Y. Wu, Y. H. Xu, S. Xing, X. X. Dai, N. Yuan and M. Y. Luo, *Spectrochim. Acta B Atom Spectrosc.*, 2021, **184**, 7.
96 S. Xing, M. Y. Luo, N. Yuan, D. Q. Liu, Y. Yang, X. X. Dai, W. C. Zhang and N. Chen, *Atom. Spectrosc.*, 2021, **42**, 62–70.
97 G. S. Yang, J. Zheng, E. Kim, S. Zhang, H. Seno, M. Kowatari, T. Aono and O. Kurihara, *Anal. Chim. Acta*, 2021, **1158**, 10.
98 W. C. Zhang, J. F. Lin, S. Fang, C. Li, X. W. Yi, X. L. Hou, N. Chen, H. T. Zhang, Y. H. Xu, H. J. Dang, W. Wang and J. Xu, *Talanta*, 2021, **234**, 9.
99 W. C. Zhang, H. T. Zhang, S. Fang, X. L. Hou, L. Y. Zhang, H. J. Dang, X. W. Yi, S. J. Zhai, W. Wang and J. Xu, *Spectrochim. Acta B Atom Spectrosc.*, 2021, **178**, 8.
100 L. C. Zhu, X. L. Hou and J. X. Qiao, *Talanta*, 2021, **221**, 9.
101 D. Zok, T. Blenke, S. Reinhard, S. Sprott, F. Kegler, L. Syrbe, R. Querfeld, Y. Takagai, V. Drozdov, I. Chyzhevskyi, S. Kirieiev, B. Schmidt, W. Adlassnig, G. Wallner, S. Dubchak and G. Steinhauser, *Environ. Sci. Technol.*, 2021, **55**, 4984–4991.
102 W. T. Bu, L. Yang, L. Tang, K. Xiong, Y. Y. Ni, C. T. Yang and S. Hu, *J. Anal. At. Spectrom.*, 2022, **37**, 1174–1178.
103 J. L. Fan, Y. F. Wang, X. F. Zhai, G. W. Chen, Z. M. Li, W. C. Zhang and T. Bai, *J. Radioanal. Nucl. Chem.*, 2022, **331**, 3025–3031.
104 A. Magre, B. Boulet, L. Pourcelot, M. Roy-Barman, A. D. Ott and C. Ardois, *J. Radioanal. Nucl. Chem.*, 2022, **331**, 4067–4076.
105 M. Matsueda, J. Aoki, K. Koarai, M. Terashima and Y. Takagai, *Anal. Sci.*, 2022, **38**, 1371–1376.
106 M. Matsueda, T. Kawakami, K. Koarai, M. Terashima, K. Fujiwara, K. Iijima, M. Furukawa and Y. Takagai, *Chem. Lett.*, 2022, **51**, 678–682.
107 Y. Y. Ni, W. T. Bu, X. T. Ding, K. Xiong, H. L. Wang, C. T. Yang, S. Hu and W. Men, *J. Anal. At. Spectrom.*, 2022, **37**, 919–928.
108 T. Ohno, N. Sato, J. Shikimori, Y. Ijichi, Y. Fukami and Y. Igarashi, *Sci. Total Environ.*, 2022, **810**, 7.
109 Y. H. Xu, C. Li, H. P. Yu, F. M. Fang, X. L. Hou, C. Zhang, X. F. Li and S. Xing, *Talanta*, 2022, **240**, 9.
110 L. Yang, W. T. Bu, K. Xiong, Y. Q. Yang and T. Z. Yang, *Spectrochim. Acta B Atom Spectrosc.*, 2022, **198**, 6.
111 W. C. Zhang, J. F. Lin, H. T. Zhang, S. Fang, C. Li, X. W. Yi, H. J. Dang, Y. H. Xu, W. Wang and J. Xu, *J. Anal. At. Spectrom.*, 2022, **37**, 1044–1052.
112 V. C. Bradley, B. W. Ticknor, D. R. Dunlap, N. A. Zirakparvar, S. C. Metzger, C. R. Hexel and B. T. Manard, *Anal. Chem.*, 2023, **95**, 15867–15874.
113 C. Carrier, A. Habibi, L. Ferreux, L. Solier, D. Hebert, C. Augeray, M. Morin, D. Maro and L. Benedetti, *J. Radioanal. Nucl. Chem.*, 2023, **332**, 2003–2015.
114 S. M. Dowell, T. S. Barlow, S. R. Chenery, O. S. Humphrey, J. Isaboke, W. H. Blake, O. Osano and M. J. Watts, *Anal. Methods*, 2023, 10, DOI: **10.1039/d3ay01030a**.
115 Z. Huang, X. L. Hou, J. X. Qiao and X. Zhao, *Talanta*, 2023, **265**, 9.
116 Z. Huang, X. L. Hou and X. Zhao, *Anal. Chem.*, 2023, 9, DOI: **10.1021/acs.analchem.3c02526**.
117 H. Jaegler and A. Gourgiotis, *J. Anal. At. Spectrom.*, 2023, **38**, 1914–1919.
118 H. Kazama, K. Konashi, T. Suzuki, S. Koyama, K. Maeda, Y. Sekio, T. Onishi, C. Abe, Y. Shikamori and Y. Nagai, *J. Anal. At. Spectrom.*, 2023, **38**, 1676–1681.
119 A. Magre, B. Boulet, A. de Vismes, O. Evrard and L. Pourcelot, *Environ. Pollut.*, 2023, **329**, 10.
120 A. Magre, B. Boulet, H. Isnard, S. Mialle, O. Evrard and L. Pourcelot, *Anal. Chem.*, 2023, **95**, 6923–6930.
121 Y. Y. Ni, W. T. Bu, K. Xiong, S. Hu, C. T. Yang and L. G. Cao, *Talanta*, 2023, **262**, 8.

122 B. C. Russell, P. E. Warwick, H. Mohamud, O. Pearson, Y. Yu, H. Thompkins, S. L. Goddard, I. W. Croudace and Z. Zacharauskas, *J. Anal. At. Spectrom.*, 2023, **38**, 97–110.
123 Y. Sakakieda, K. Hosokawa, F. Nakanishi, Y. Hino, Y. Inome, A. Sakaguchi, Y. Takaku, S. Yamasaki, K. Sueki, M. Ikeda and H. Sekiya, *Prog. Theor. Exp. Phys.*, 2023, **2023**, 103H01.
124 K. Xiong, W. T. Bu, Y. Y. Ni, X. M. Liu, J. Zheng, T. Aono, C. T. Yang and S. Hu, *Microchem. J.*, 2023, **190**, 7.
125 G. S. Yang, E. Kim, H. Seno, M. Kowatari and O. Kurihara, *J. Radioanal. Nucl. Chem.*, 2023, 9, DOI: **10.1007/s10967-023-09240-5**.
126 Y. Yang, M. Y. Luo, Y. Wu, N. Yuan, J. J. He, H. M. Guo and Q. An, *J. Environ. Radioact.*, 2023, **270**, 9.
127 A. D. French, K. M. Melby, K. P. Hobbs, R. M. Cox, G. Eiden, E. W. Hoppe, I. J. Arnquist and K. Harouaka, *Talanta*, 2024, **272**, 9.
128 K. P. Hobbs, A. D. French, K. M. Melby, E. J. Bylaska, K. Harouaka, R. M. Cox, I. J. Arnquist and C. L. Beck, *Anal. Chem.*, 2024, **96**, 5807–5814.
129 K. Ichimura, K. Chiba, Y. Gando, H. Ikeda, Y. Kishimoto, M. Kurasawa, K. Nemoto, A. Sakaguchi, Y. Takaku and Y. Sakakieda, *Prog. Theor. Exp. Phys.*, 2024, **2024**, 063H01.
130 T. J. Kell and S. V. Jovanovic, *J. Radioanal. Nucl. Chem.*, 2024, 6, DOI: **10.1007/s10967-023-09317-1**.
131 C. Y. Peng, J. Sun, F. Zhang, S. Xing, X. C. Liu, C. C. Chen, X. L. Hou, K. L. Shi and W. S. Wu, *Anal. Chem.*, 2024, **96**, 2514–2523.
132 J. C. Tremblay-Cantin, L. Martin, M. Proulx, N. D. Priest and D. Larivière, *J. Environ. Radioact.*, 2024, **274**, 11.
133 W. Wang, J. Xu, R. Y. Xi, S. Q. Guo, Y. Y. Su, S. Fang, H. T. Zhang, Y. L. Wang, J. L. Fan, L. Feng, Y. F. Wang and Z. M. Li, *J. Anal. At. Spectrom.*, 2024, **39**, 178–189.
134 Y. C. Wang, M. T. Zhang and X. L. Hou, *Chin. J. Anal. Chem.*, 2024, **52**, 706–716.
135 T. Ohno, Y. Muramatsu, Y. Shikamori, C. Toyama, N. Okabe and H. Matsuzaki, *J. Anal. At. Spectrom.*, 2013, **28**, 1283–1287.
136 G. Yang, H. Tazoe and M. Yamada, *Anal. Chim. Acta*, 2018, **1008**, 66–73.
137 G. S. Yang, H. Tazoe, E. Kim, J. Zheng, M. Kowatari and O. Kurihara, *J. Anal. At. Spectrom.*, 2023, **38**, 2562–2570.
138 C. Coralie, H. Azza, A. Michelle, A. Celine, B. Didier, M. Denis and B. Lucilla, *J. Anal. At. Spectrom.*, 2022, **37**, 1309–1317.
139 F. Stäger, D. Zok, A. K. Schiller, B. Feng and G. Steinhauser, *Environ. Sci. Technol.*, 2023, **57**, 13601–13611.
140 Ä. Zacharauskas, P. Warwick, B. Russell, D. Reading and I. Croudace, *J. Anal. At. Spectrom.*, 2023, **38**, 1431–1441.
141 Y. B. Zhu and D. Asakawa, *iScience*, 2024, **27**, 111138.
142 A. Ebeling, T. Zimmermann, O. Klein, J. Irrgeher and D. Pröfrock, *Geostand. Geoanal. Res.*, 2022, **46**, 351–378.
143 S. V. Jovanovic and T. Kell, *J. Radioanal. Nucl. Chem.*, 2021, **329**, 319–326.
144 H. Kominami and Y. Suzuki, *Bunseki Kagaku*, 2017, **66**, 825–837.
145 R. Mortazavi, S. Attiya and P. A. Ariya, *Sci. Total Environ.*, 2019, **690**, 277–289.
146 A. Przibilla, S. Iwainski, T. Zimmermann and D. Pröfrock, *Water Environ. Res.*, 2023, **95**, e10922.
147 A. Reese, T. Zimmermann, D. Pröfrock and J. Irrgeher, *Sci. Total Environ.*, 2019, **668**, 512–523.
148 M. Sojka, A. Choinski, M. Ptak and M. Siepak, *Sci. Rep.*, 2021, **11**, 244.
149 M. Sojka, A. Choinski and M. Siepak, *Land Degrad. Dev.*, 2024, **35**, 3407–3421.
150 M. Sojka, M. Siepak and K. Pietrewicz, *J. Elementol.*, 2019, **24**, 125–140.
151 C. Telloli, F. Cicconi, E. Manzi, F. Borgognoni, S. Salvi, M. C. Iapalucci and A. Rizzo, *Food Chem.*, 2024, **450**, 139370.
152 S. Trimmel, T. C. Meisel, S. T. Lancaster, T. Prohaska and J. Irrgeher, *Anal. Bioanal. Chem.*, 2023, **415**, 1159–1172.
153 T. Zimmermann, M. von der Au, A. Reese, O. Klein, L. Hildebrandt and D. Pröfrock, *Anal. Methods*, 2020, **12**, 3778–3787.
154 Z. T. Wang, J. Zheng, Y. Y. Ni, W. Men, K. Tagami and S. Uchida, *Anal. Chem.*, 2017, **89**, 2221–2226.
155 N. Suguyama and K. Nakano, *Reaction Data for 70 Elements Using O2 , NH3 and H2 Gases with the Agilent 8800 Triple Quadrupole ICP-MS*, Report 5991-4585EN, 2014.
156 S. T. Lancaster, T. Prohaska and J. Irrgeher, *J. Anal. At. Spectrom.*, 2023, **38**, 1135–1145.
157 Y. B. Zhu, *Chem. Commun.*, 2024, **60**, 3974–3977.
158 Y. B. Zhu and A. Itoh, *Anal. Chim. Acta*, 2021, **1180**, 338854.
159 J. Zheng and M. Yamada, *Talanta*, 2006, **69**, 1246–1253.
160 A. Held and P. D. P. Taylor, *J. Anal. At. Spectrom.*, 1999, **14**, 1075–1079.
161 R. Muragan, N. Veerasamy, Y. Zhao, T. Aono and S. K. Sahoo, *Int. J. Mass Spectrom.*, 2021, **467**, 116623.
162 V. C. Bradley, T. M. Weilert and J. D. Brockman, *Talanta*, 2021, **221**, 121622.
163 N. T. Hubley, J. D. Brockman and J. D. Robertson, *Radiochim. Acta*, 2017, **105**, 629–635.
164 N. T. Hubley, D. L. Wegge, T. M. Weilert, C. P. Leibman, M. S. Rearick, J. D. Robertson and J. D. Brockman, *J. Radioanal. Nucl. Chem.*, 2018, **318**, 49–54.
165 C. A. Mason, N. T. Hubley, J. D. Robertson, D. L. Wegge and J. D. Brockman, *Radiochim. Acta*, 2017, **105**, 1059–1070.
166 M. J. O'Hara, C. M. Kellogg, C. M. Parker, S. S. Morrison, J. F. Corbey and J. W. Grate, *Chem. Geol.*, 2017, **466**, 341–351.
167 G. Ujvári, U. Klötzli, M. Horschinegg, W. Wegner, D. Hippler, G. I. Kiss and L. Palcsu, *Rapid Commun. Mass Spectrom.*, 2021, **35**, e9081.
168 H. Wang, Y. Y. Ni, J. Zheng, Z. Y. Huang, D. T. Xiao and T. Aono, *Anal. Chim. Acta*, 2019, **1050**, 71–79.
169 Y. Okazaki, S. Hoshi, T. Kato, T. Fukui, K. Toda and S. I. Ohira, *ACS Omega*, 2022, **7**, 14082–14088.
170 Y. Sugo, R. Miyachi, Y. H. Maruyama, S. I. Ohira, M. Mori, N. S. Ishioka and K. Toda, *Anal. Chem.*, 2020, **92**, 14953–14958.